Pressure-induced symmetry changes in body-centred cubic zeolites

A. Nearchou,[a] M. U. Cornelius,[b] Z. L. Jones,[a] I. E. Collings,[c] S. A. Wells,[d] P. R. Raithby[a] and A. Sartbaeva[a]

[a] *University of Bath, Department of Chemistry, Claverton Down, Bath, BA2 7AY, UK*
[b] *University of the Western Cape, Department of Chemistry, Bellville, Cape Town, 7535, South Africa*
[c] *European Synchrotron Radiation Facility, 71 avenue des Martyrs, 38000, Grenoble, France*
[d] *University of Bath, Department of Chemical Engineering, Claverton Down, Bath, BA2 7AY, UK*

Abstract

Previous work has shown a strong correlation between zeolite framework flexibility and the nature of structural symmetry and phase transitions. However, there is little experimental data regarding this relationship, in addition to how flexibility can be connected to the synthesis of these open framework materials. This is of interest for the synthesis of novel zeolites, which require organic additives to permutate the resulting geometry and symmetry of the framework. Here, we have used high pressure powder X-ray diffraction to study the three zeolites: Na-X, RHO and ZK-5, which can all be prepared using 18-crown-6 ether as an organic additive. We observe significant differences in how the occluded 18-crown-6 ether influences the framework flexibility – this being dependant on the geometry of the framework. We use these differences as an indicator to define the role of 18-crown-6 ether during zeolite crystallisation. Furthermore, in conjunction with previous work we predict that pressure-induced symmetry transitions are intrinsic to body-centred cubic zeolites. The high symmetry yields fewer degrees of freedom, meaning it is energetically favourable to lower the symmetry to facilitate further compression.

Introduction

Zeolites are a class of microporous aluminosilicates, recognised for possessing periodic open-framework structures. On the molecular-level, zeolites are built from corner-sharing tetrahedra of the form TO_4, where the T atoms are Si or Al. From a topological perspective, these primary tetrahedra arrange into regular geometric cages and rings, which are referred to as secondary building units (SBUs).[1,2] Due to the presence of tetracoordinated aluminium, the framework retains a net negative charge, which is counter-balanced by mobile metal cations dispersed throughout the framework. Although conventional solid-state chemistry considers solids as static materials, zeolite frameworks demonstrate an inherent flexibility.[3-7] Although the TO_4 tetrahedral units are rigid, the T-O-T bridging angles possess significant freedom, permitting the framework to contract or expand as a response to thermodynamic stimuli.[1,8] Such low frequency dynamics can result in distortions of the underlying SBUs and in some cases alterations in symmetry.

Little research is reported on the low frequency modes and elastic behaviour of zeolites under compression. This is unfortunate, as such research is shown to be beneficial in understanding how atomic scale topological structure can dictate physical properties. A prime instance of this is expressed by the family of fibrous zeolites, specifically edingtonite, natrolite, thomsonite and scolecite.[9,10] All four zeolites display anisotropic elastic behaviour, which is dictated by the anti-rotation of the SBU chains present in their structures. The nature of how geometry and SBUs influence elastic behaviour has been explored through the concept of *the flexibility window*.[3] This being the range of densities at which the framework can exist where the connectivity is retained and

the TO_4 tetrahedral units remain rigid and undeformed. Use of the flexibility window has proven to explain pressure-induced phase transitions,[11-13] in addition to being a potential criterion to rationally design novel zeolites.[5]

In addition, high pressure studies provide scope for alternative preparation routes to novel zeolites, via reconstructive phase transitions.[14] However, several zeolites express pressure-induced phase transitions that do not require disassembly of the framework. Such transitions appear to be more intrinsic to the geometry of the framework. Such an example is zeolite RHO, which possesses an ambient centric space group of $Im\bar{3}m$ that evolves into the acentric $I\bar{4}3m$ space group with the application of pressure.[15-17] This is characterised by the increasing ellipticity of the 8-ring openings in the framework, as shown in figure 1. This phase transition has also been observed with specific dehydration and heating conditions.[18,19] Another example concerns ANA-type zeolites, of which the materials analcime,[20] leucite,[21] pollucite[22] and wairakite[23] all show pressure-induced reductions in symmetry to a triclinic system. Such phase transitions have shown good agreement with the flexibility window property,[12,24] whereby the transitions are defined and facilitated by the nature of the topological geometry. Interestingly, for both RHO and ANA-type zeolites, the data consistently demonstrate that the higher pressure polymorph is more compressible.[16,20-23]

The mechanical behaviour of zeolites is also strongly influenced by the presence of extra-framework content and the pressure transmitting medium used. These media are characterised as *penetrating* and *non-penetrating* fluids,[10] whereby use of penetrating fluid typically increases the mechanical stiffness due to increased extra-framework content.[25-28] These observations are a result of the pressure-transmitting medium occupying the pores of the framework structure, and essentially preventing structural collapse. This is evident from both experimental behaviour[11] and the simulated flexibility window of zeolites.[29] The importance of considering such framework content is emphasised by the over-hydration effect, whereby non-framework content such as water is being forced into the framework with the application of pressure.[30-32] Consequently, this leads to a decrease in compressibility as a function of pressure. However, recent simulations by Fletcher et al.[33] have shown how the intrinsic flexibility window of the EMT framework is unperturbed by the occlusion of 18-crown-6 ether (18C6). This is of particular interest, as 18C6 is used as an organic additive in the preparation EMT-type zeolites like EMC-2,[34,35] where synthesis without 18C6 has not been achieved.[36] Therefore, Fletcher et al. suggest from their findings that 18C6 may not necessarily behave as a true geometric template, but rather influence the free-energy landscape of crystallisation. This highlights how the study of framework flexibility can provide valuable insights into the nature of zeolite synthesis.

Figure 1 shows the framework structure of the cubic zeolites Na-X, RHO and ZK-5. Like zeolite EMC-2, all three can be prepared using 18C6 as an organic additive.[35] In zeolite Na-X the 18C6 molecule occupies the *t-fau* supercage, whereas in RHO and ZK-5 it occupies the α-cage. Both zeolites Na-X and RHO have been investigated under high pressure,[15-17,26,37] with the latter displaying the aforementioned phase transition. However, zeolite ZK-5, which is topologically analogous to zeolite RHO, has not been studied previously as far as we know. In addition to this, the influence of the occluded 18C6 on the framework dynamics have likewise not been studied for all three zeolites. Herein, we report for the first time, experimental high pressure data for zeolite ZK-5, in addition to the as-synthesised zeolites Na-X, RHO and ZK-5 with 18C6 occluded in the framework cavities. From these data, we have gleaned insights into the role of 18C6 in the crystallisation of these three zeolites. Furthermore, we propose that pressure-induced changes in symmetry are an intrinsic feature to body-centred cubic zeolites. Such reductions in symmetry are favourable as they facilitate

further compression without deformation of the framework tetrahedra, preventing 'early onset' pressured-induced amorphisation.

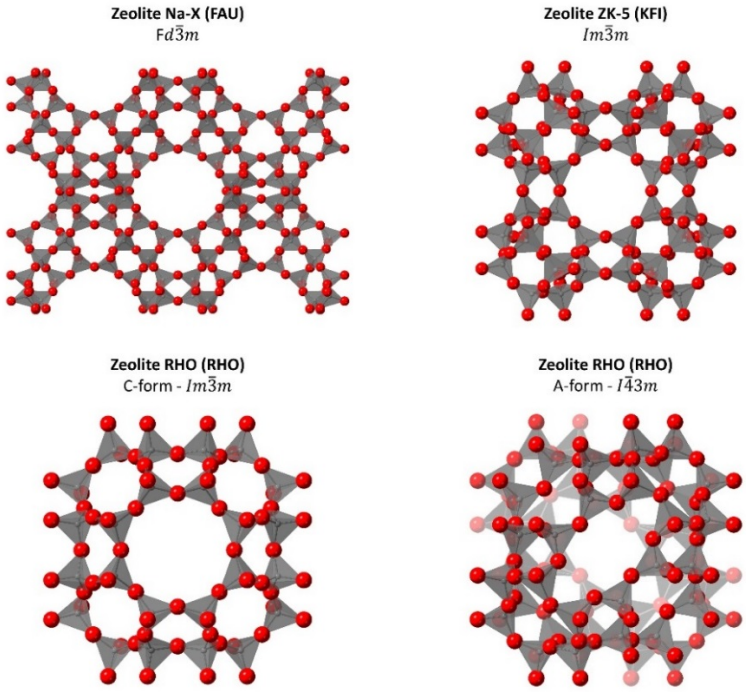

Figure 1. The structures and space groups of zeolites Na-X, ZK-5 and the C and A-forms of zeolite RHO. The framework topology is indicated in parentheses. Oxygen atoms are shown as red spheres, and SiO_4 tetrahedra as translucent solids.

Experimental

Sample Preparation

The zeolite Na-X, RHO and ZK-5 samples used in the high pressure analysis were synthesised following the procedures used by Chatelain et al.[35,38,39] The molar batch compositions of the precursor hydrogel for each synthesis is shown in table 1. The materials used were sodium hydroxide (NaOH), potassium hydroxide (KOH), caesium hydroxide solution (50 wt% CsOH in water), strontium nitrate ($Sr(NO_3)_2$), 18-crown-6 ether ($C_{12}H_{24}O_6$ 18C6), sodium aluminate ($NaAlO_2$), aluminium hydroxide ($Al(OH)_3$), colloidal silica (LUDOX® HS-40, 40 wt% SiO_2 in water) and distilled water. All materials were purchased from Sigma-Aldrich.

Table 1. Hydrogel batch compositions used in the preparation of zeolites Na-X, RHO and ZK-5

Zeolite	Al_2O_3	Na_2O	K_2O	Cs_2O	SrO	SiO_2	18C6	H_2O
Na-X	1	2.9				10	0.5	90
RHO	1	1.8		0.3		10	0.5	100
ZK-5	1		2.7		0.1	10	1.0	220

Zeolite Na-X

In a Naglene Teflon FEP bottle, the sodium hydroxide and 18C6 were dissolved in the distilled water. The sodium aluminate was subsequently added to the solution and stirred until homogeneous. Next

the colloidal silica was slowly added to the solution while stirring, to avoid rapid gelation. The hydrogel was then aged for 4 hours under ambient conditions, before being sealed and the bottle placed into a 100°C oven for 8 days. Upon the completion of crystallisation, the bottle was removed from the oven, cooled and the product separated from the mother liquor using Buchner filtration. The product was washed with distilled water, until the filtrate was of neutral pH. The product powder was subsequently dried and ground until sample calcination and dehydration.

Zeolite RHO

The sodium hydroxide and 18C6 were dissolved in the distilled water and caesium hydroxide solution. Upon dissolution, the sodium aluminate was added, and left to stir until the solution was homogeneous. Following this, the colloidal silica was poured into the solution slowly so as not to produce a viscous gel. The formed hydrogel was then aged for 24 hours under stirring at ambient conditions. After aging, the gel was transferred to a Teflon cup within a sealed stainless steel autoclave. The hydrogel containing autoclave was subsequently placed into a 110°C oven for 8 days. After this time the autoclave was removed from the oven, cooled and opened. The product was removed from the mother liquor using Buchner filtration, and washed with distilled water until the filtrate was of neutral pH. The washed powder was then dried and ground until sample calcination and dehydration.

Zeolite ZK-5

Within a conical flask, the potassium hydroxide was dissolved in distilled water. The aluminium hydroxide was added to this solution and the flask weighed. The solution was then heated to near 110°C under stirring. Upon dissolution of the aluminium hydroxide, the solution was cooled, weighed and any water lost during heating topped up with additional water. In a separate beaker, the strontium nitrate and 18C6 were dissolved in a small amount of water, followed by the colloidal silica, ensuring the solution was homogeneous. Subsequently, the alumina solution was quickly added to the silica solution under stirring, to form the hydrogel. The hydrogel was stirred for 30 minutes, to ensure it was thoroughly mixed.

The gel was then transferred to a Teflon cup within a sealed stainless steel autoclave. Next, the autoclave was placed into a 150°C oven for 5 days. Upon complete crystallisation at this time, the autoclave was removed from the oven and allowed to cool. The crystalline product was then separated from the mother liquor via Buchner filtration, and washed until the filtrate was of neutral pH. The product was then dried and suitably ground until sample calcination and dehydration.

Calcination and Dehydration

The filled (18C6 containing) and empty (calcined) analogues of each zeolite were prepared from the same sample that was separated into two.

To prepare the empty analogue of each zeolite, half of the sample was calcined in air. The powder was heated at a ramp rate of 1 $Kmin^{-1}$ to 100°C, 200°C and 300°C for 1 hour and finally 450°C for 6 hours. After calcination the sample was cooled at a rate of 1 $Kmin^{-1}$, stopping at 200°C for 1 hour and terminating at ambient temperature.

The calcined and as-synthesised analogue of each zeolite was next dehydrated under vacuum. The samples were heated at a ramp rate of 1 $Kmin^{-1}$, holding at 100°C for 1 hour and 200°C for 6 hours. After dehydrating at 200°C, the sample was cooled at a rate of 1 $Kmin^{-1}$, stopping at 100°C for 1 hour and terminating at ambient temperature.

High Pressure X-ray Diffraction

The zeolite powder samples were analysed using high pressure X-ray diffraction on the ID15B beamline at the European Synchrotron Radiation Facility (ESRF) in Grenoble, France. The samples were loaded into diamond anvil cells (DACs) alongside a ruby chip, using Daphne 7373 oil as a non-penetrating pressure transmitting medium. The applied pressure in the DAC was determined by the shift of the R1 emission line of the ruby fluorescence.[40] The incident synchrotron X-ray radiation used in the experiment was of wavelength 0.4113 Å, and the detector parameters were calibrated using silicon. At sequential steps of increasing pressure a diffraction pattern was taken, with the pressure being recorded before and after each pressure step to provide an average pressure throughout the measurement. The samples were compressed until complete pressure-induced amorphisation was imminent. The DACs were then depressurised, with several diffraction patterns measured upon the decompression cycle to ambient conditions.

Three diffraction images were taken at each pressure point, which were used to produce an average image using the FIT2D software.[41] Subsequently, the Dioptas software was used to integrate the 2D area images into 1D powder diffraction patterns.[42] To determine the unit cell parameters at each pressure, Pawley refinements of the diffraction patterns were achieved using the TOPAS Academic software.[43] The sequential refinements with increasing pressure were performed using the Batch mode. Zeolite Na-X was refined to the $Fd\bar{3}m$ space group. The C and A-forms observed in zeolite RHO were refined to the $\mathfrak{I}\bar{3}m$ and $I\bar{4}3m$ space groups, respectively. The cubic and tetragonal phases of zeolite ZK-5 were refined to space groups $\mathfrak{I}\bar{3}m$ and $I4/mmm$, accordingly.

The flexibility windows of the empty and filled zeolite frameworks were determined using the GASP software developed by Wells.[44,45] The bulk moduli of the zeolite samples were calculated in the PASCal webtool by Cliffe and Goodwin.[46] Only unit cell data within the 0-2.2 GPa range were used, and fitted to the 2nd and 3rd order Birch-Murnaghan equations of state, depending on which equation showed the best fit. The fits were weighted with the 0.1 GPa error in pressure determination.

Results

Zeolite Na-X

The unit cell parameter *a* as a function of pressure for the calcined (empty) and 18C6 containing (filled) zeolite Na-X are shown in figures 2a and 2b accordingly. In both samples the cell parameter contracts linearly with pressure, but displays a small decrease in gradient after approximately 2.2 GPa. This change in gradient is likely a consequence of the Daphne 7373 oil solidifying.[47]

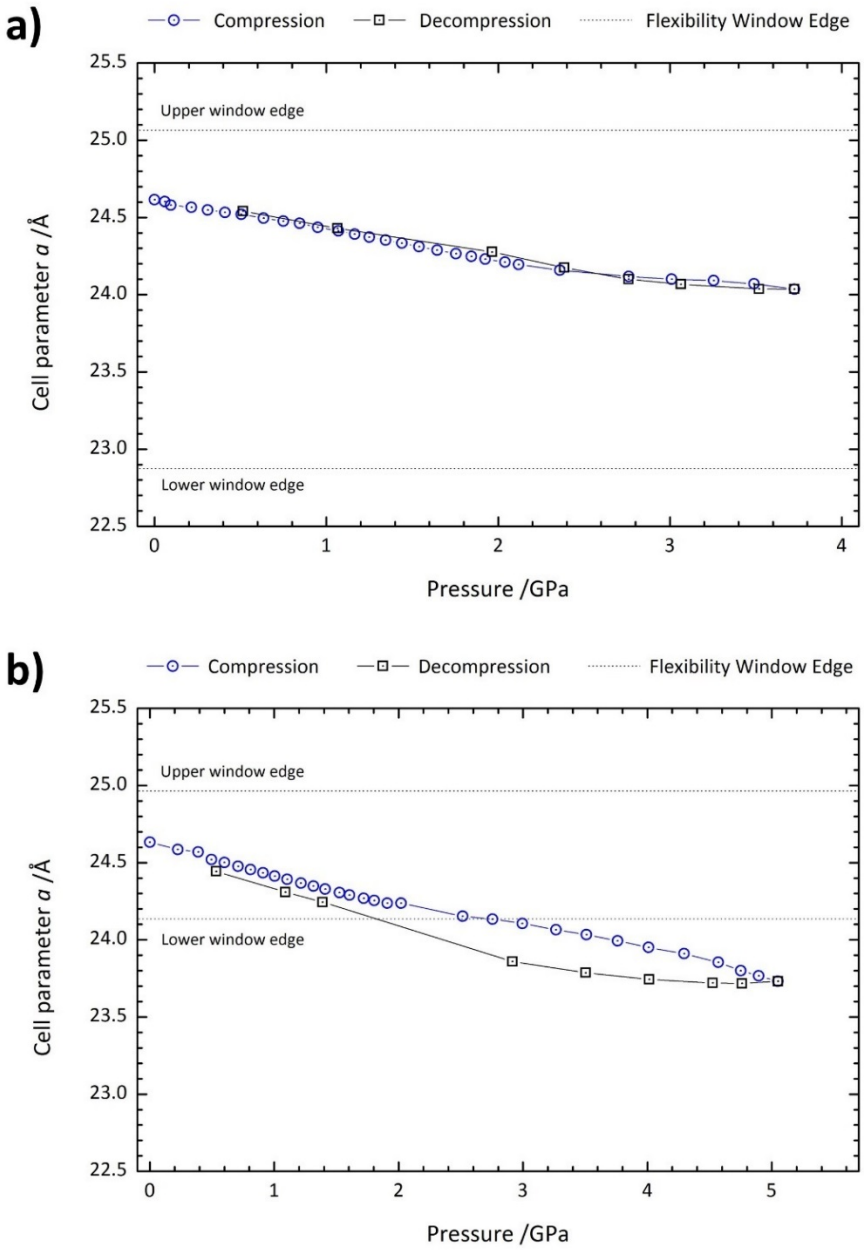

Figure 2. Cell parameter *a* as a function of pressure for a) the empty and b) the filled zeolite Na-X. Blue circle data points correspond to the compression cycle, and black squares to the decompression. Also shown are the edges of the flexibility window as simulated in the GASP software.

The empty zeolite Na-X was compressed to 3.8 GPa, where the onset of pressure-induced amorphisation was imminent. Upon decompression, we observed that the unit cell expanded following the same pathway observed with contraction. Throughout the entirety of the experiment the empty zeolite remained within the flexibility window, indicating that there were no deformations of the rigid tetrahedra. Furthermore, this demonstrates the intrinsic reversible mobility of the framework with compression and decompression within the studied pressure range.

As for the filled zeolite Na-X, the simulated flexibility window is substantially narrowed. This demonstrates that the steric bulk of the 18C6 molecule theoretically restricts the extent to which the

framework tetrahedra can move. The experimental data illustrates that the zeolite leaves the confines of the flexibility window, suggesting that the framework tetrahedra are distorted above approximately 2.8 GPa. The filled sample was compressed to 5.1 GPa, and with subsequent decompression we observed a hysteresis in the expansion of the unit cell. Such a delay in expansion during the decompression cycle can be due to two possibilities. The first is that the pressure experienced by the filled zeolite could be higher than what was recorded, indicating greater non-hydrostatic stress compared to the empty zeolite. The second possibility concerns the potentially distorted framework tetrahedra. During the decompression, these tetrahedra take longer to reassert their ideal tetrahedral geometry, alongside the crystal periodicity. This observation agrees with work by Huang et al.[48] and Havenga et al.[49] which report FAU-type zeolites can express 'structural memory', whereby the extra-framework content permit reversible amorphisation.

Figure 3 displays the comparison in unit cell volume contraction with pressure for the empty and filled zeolite Na-X samples. It can be seen that the filled zeolite Na-X was capable of being compressed to a higher pressure, showing a slower decline of crystallinity with pressure. This indicates that the 18C6 molecule is enhancing the structural integrity of the FAU framework, improving the resistance to pressure-induced amorphisation. Such a trend has been reported previously with extra-framework content in the channels of other zeolites.[11,13]

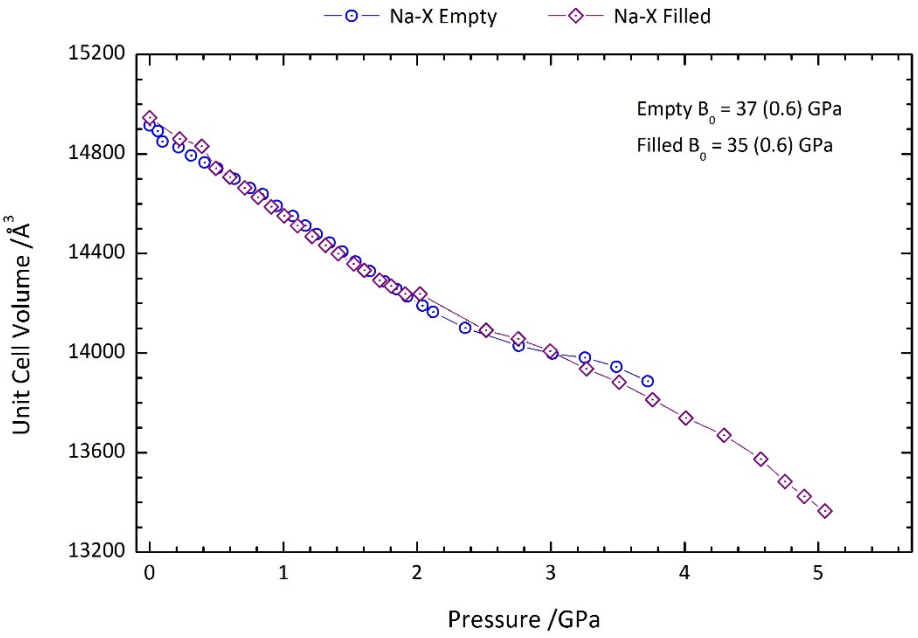

Figure 3. The variation of cell volume with increasing pressure for zeolite Na-X. The empty analogue is shown with blue circles, and the filled with purple diamonds. Also included are the bulk moduli (B_0) of the two zeolites, using the Birch-Murnaghan 2nd order fit calculated using the PASCal webtool, as shown in the SI.

Also shown in figure 3 are the calculated bulk moduli of 37 and 35 GPa for the empty and filled zeolite Na-X samples respectively. These values demonstrate that the mechanical compressibility of the FAU framework is not impeded by the presence of the 18C6 molecule in the *t-fau* supercage. This is substantiated by the observation that both samples show a comparable unit cell contraction with pressure. We propose that although the 18C6 molecule has steric bulk, it has inherent molecular flexibility, meaning it can bend in response to the collapse of the supercage. This mirrors the predictions of Fletcher et al.[33] from GASP geometric simulations of the EMT framework containing

the 18C6 molecule. However, there is a discrepancy as the flexibility of the filled and empty EMT frameworks are identical, unlike that seen herein for the FAU framework. It is anticipated that the spherical supercage in the FAU frameworks contracts to a size whereby the 18C6 molecule can no longer flex, and its steric bulk begins to interfere with the mobility of the framework.

The bulk moduli reported herein for zeolite Na-X agree with the anticipated range for open framework silicates (15-70 GPa),[25] and are comparable to the value reported by Colligan et al.[26] for purely siliceous zeolite Y. The similarity in the bulk modulus for zeolites Na-X and Y suggests that the framework Si/Al ratio has little influence on the material's compressibility.

Zeolite RHO

Concerning zeolite RHO, the diffraction patterns for both the empty and filled samples exhibited Bragg peak doubling with the application of pressure. Doubling was observed at 0.2 GPa, with a coexistence of two phases up to 1.1 GPa. This doubling corresponds to the transition from the ambient C-form of $Im\bar{3}m$ symmetry to the A-form of $I\bar{4}3m$ symmetry, as has been seen previously.[15-17] As mentioned, this transition is characterised by the elliptical distortion of the 8-ring openings in the RHO framework. The presence of the 18C6 molecule does not influence the onset or offset of the symmetry change.

Figure 4a and 4b illustrate the variation in cell parameter *a* with pressure for the empty and filled zeolite RHO accordingly. These figures include the cell parameters for both the C and A-forms observed, in addition to the edges of their respective flexibility windows simulated using the GASP software. As with zeolite Na-X, both the filled and empty samples of zeolite RHO express a change in gradient at approximately 2.2 GPa, due to the solidification of the pressure transmitting medium.[47]

Concerning the empty zeolite, both the C and A-forms exists well within the confines of their flexibility windows, demonstrating that there is no distortion of the framework tetrahedra. The placement of the C-form window edges illustrate that the distortion in the A-form permits greater framework mobility that satisfies the rigidity of the tetrahedra. This is due to the reduced symmetry. With decompression, the unit cell expands following the same pathway as the compression, indicating that there is no impedance to the framework mobility from the exerted pressure. Furthermore, the zeolite returns to the ambient C-form with no apparent hysteresis, indicating that the symmetry change is fully reversible.

The reversibility of the symmetry change is also observed for the filled zeolite RHO. Moreover, although the filled sample appears to just leave the flexibility window, the unit cell expansion follows the same pathway as the compression cycle. This indicates that if the framework tetrahedra are distorted at the highest pressure, it is not substantial enough to result in a hysteresis with decompression.

For the ambient C-form there is an apparent expansion of the window, indicating that the presence of the 18C6 molecule is improving the flexibility of the framework. This is corroborated by the unusual behaviour observed from the experimentally determined bulk moduli, shown in figure 5. Here it is shown that the filled C-form of zeolite RHO is significantly more compressible than the empty equivalent. This contrasts typical behaviour, whereby the presence of extra-framework content reduces the zeolite material's softness.[25] Herein, it is understood that due to geometric constraints the framework tetrahedra are effectively moving around the 18C6 molecule with

enhanced mobility. This observation of enhanced compressibility with the addition of extra-framework content in zeolites has not been reported previously.

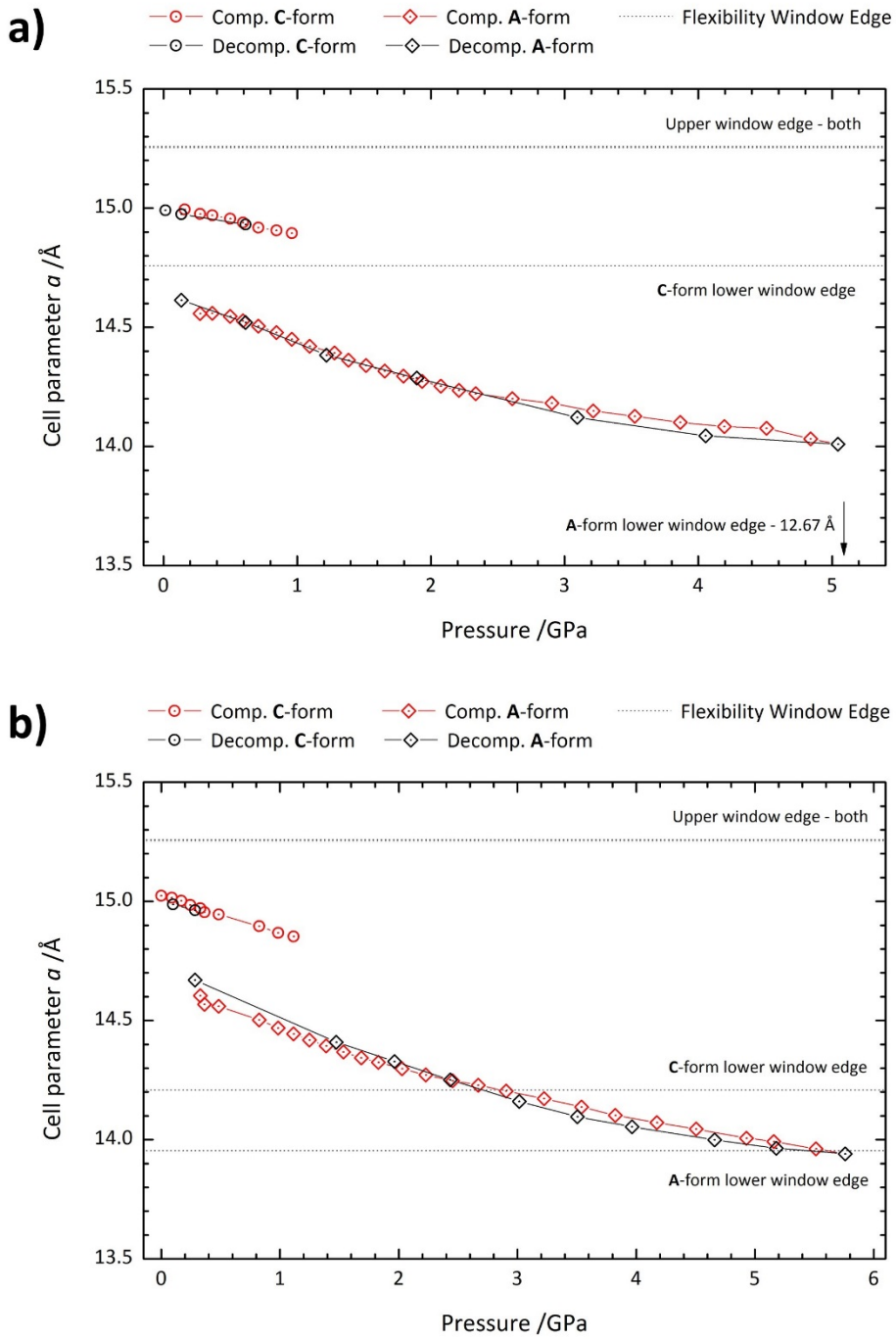

Figure 4. Cell parameter *a* as a function of pressure for a) the empty and b) the filled zeolite RHO. Red data points correspond to the compression cycle, and black to the decompression. Circles correspond to the ambient C-form, and diamonds to the A-form. Also shown are the edges of the flexibility window as simulated in the GASP software.

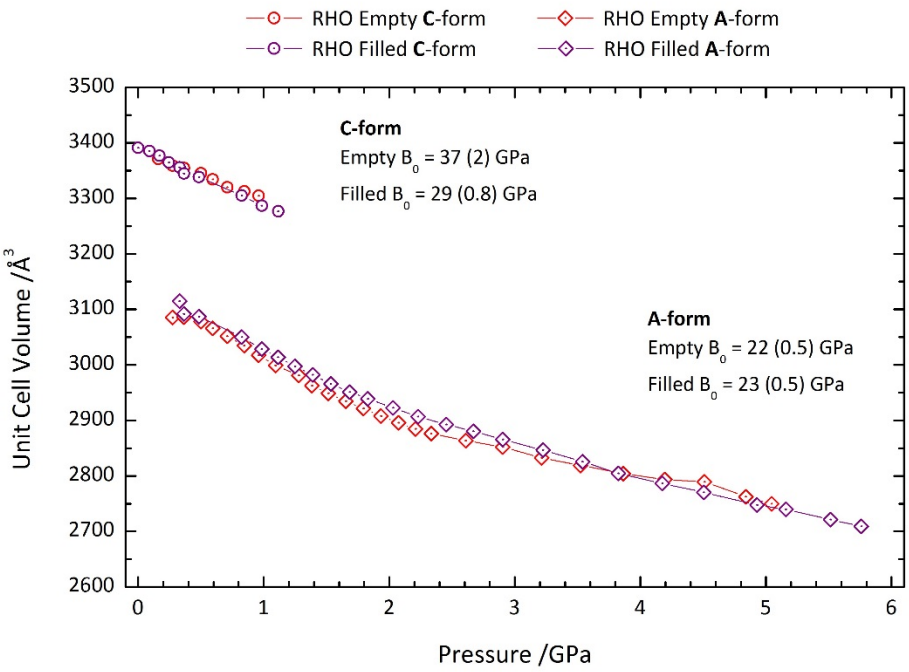

Figure 5. The variation of cell volume with increasing pressure for zeolite RHO. The empty analogue is shown in red, and the filled in purple. Circle data points correspond to the C-form, and diamonds to the A-form. Also included are the bulk moduli (B_0) of the two forms of the zeolites, using the Birch-Murnaghan 2nd order fit calculated using the PASCal webtool, as shown in the SI.

Occupation of the α-cage by the 18C6 is seen to contract the higher density edge of the flexibility window for the lower symmetry A-form. This is to be expected, as it is the steric bulk of the 18C6 molecule which is restricting the extent to which the framework tetrahedra can collapse into the α-cage. Figure 5 displays the unit cell contraction with pressure, illustrating a good agreement between the empty and filled analogues of the A-form. This is substantiated by the congruence in the bulk moduli of these two samples. Furthermore, it demonstrates that with the decrease in the cubic symmetry, the 18C6 molecule is capable of flexing to accommodate the contraction of the framework. Such behaviour mirrors that observed for zeolite Na-X.

Zeolite ZK-5

Compression of zeolite ZK-5 yielded splitting in most of the Bragg peaks from 1.5 GPa onwards for both the empty and filled samples. Bragg peaks where *h, k* and *l* values of the Miller index are equivalent did not express splitting. Such behaviour was attributed to a phase transition to a tetragonal symmetry. This phase was indexed and refined to the $I4/mmm$ space group, and characterised by a contraction of cell parameter *c* relative to cell parameters *a* and *b*. The pressure at which the symmetry change occurs was not observed to be influenced by the occlusion of the 18C6 molecule within the framework. Figure 6 shows the GASP simulated structures of the empty zeolite ZK-5 at 0.0 and 3.0 GPa in the cubic and tetragonal symmetries respectively. This highlights how the tetragonal phase is characterised by a contraction along the *c* axis, in addition to the circular 8-ring openings becoming elliptical. This increasing ellipticity of the 8-ring openings is also observed for zeolite RHO from transitioning from the C to the A-form as discussed earlier.

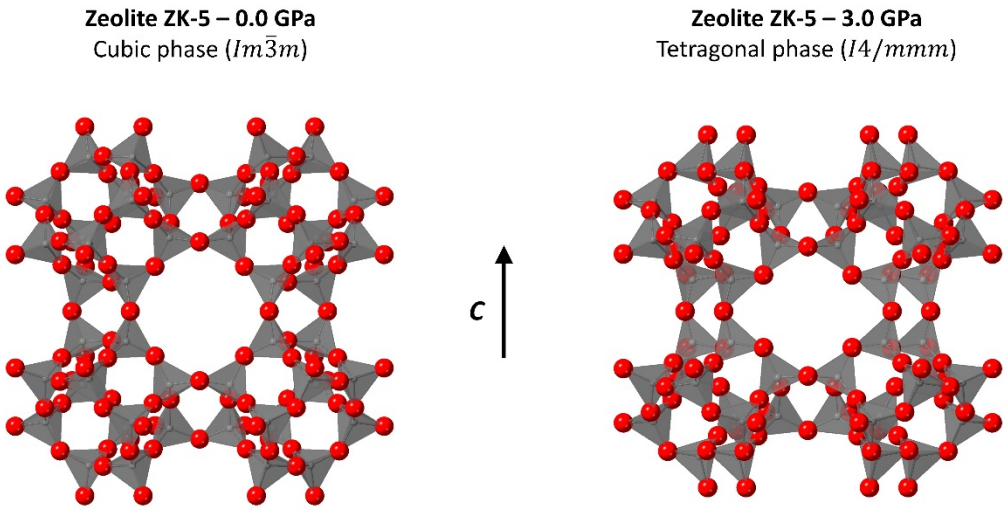

Figure 6. Unit cell structures of empty zeolite ZK-5 at pressures of 0.0 (cubic) and 3.0 GPa (tetragonal). Simulated in the GASP software using the cell parameters determined from the diffraction data. Oxygen atoms are shown as red spheres, and SiO_4 tetrahedra as translucent solids.

Figures 7a and 7b display the variation in unit cell dimensions for the empty and filled zeolite ZK-5 samples observed throughout the compression. These figures include the unit cell dimensions for both the cubic and tetragonal phases of the sample, alongside their respective flexibility windows simulated using the GASP software. For both samples, the cubic and tetragonal phases were observed within the confines of their simulated windows, indicating no pressure-induced distortions of the framework tetrahedra.

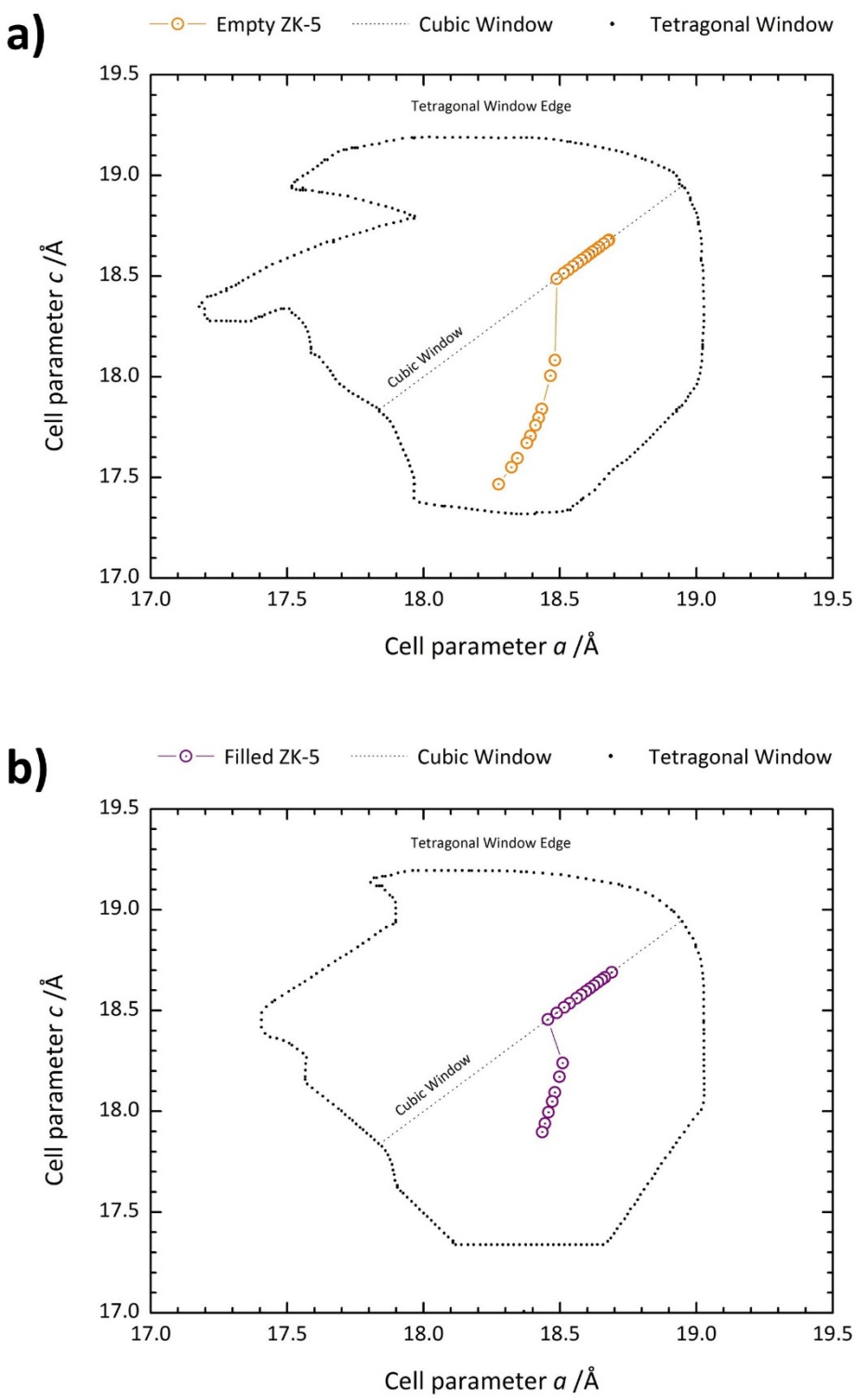

Figure 7. Unit cell dimensions of the a) empty and b) filled zeolite ZK-5 throughout compression. Also shown are the extents of the corresponding flexibility windows, as simulated using the GASP software. The black dots display the edge of the tetragonal window, and the fine dashed line the pathway of the cubic window.

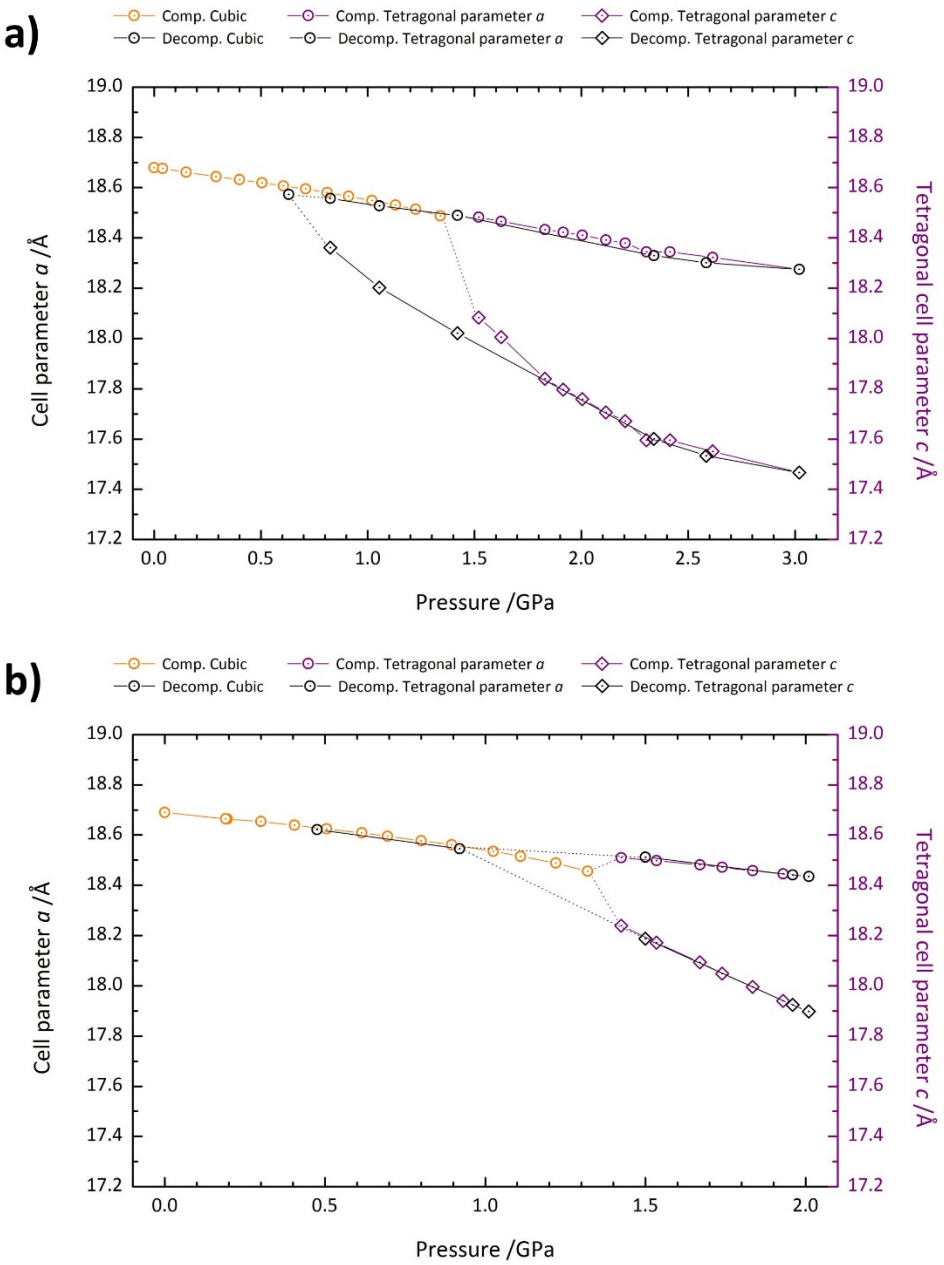

Figure 8. Cell parameter *a* and tetragonal cell parameter *c* as a function of pressure for a) the empty and b) the filled zeolite ZK-5. Circles correspond to the *a* parameter, and diamonds to the tetragonal *c* parameter. Data points shown in orange refer to the cubic phase, purple the tetragonal phase and black to the decompression cycle of both phases. The dotted lines indicate the cell parameter shift between the two phases.

With regards to the windows, the tetragonal window displays some narrowing with the occupation of the α-cage in the KFI framework by the 18C6 molecule. This is to be expected and has been expressed herein by zeolite Na-X and the A-form of zeolite RHO. The reasoning being the same, whereby the steric bulk of the 18C6 molecule is preventing the framework tetrahedra from collapsing into the cavity. Alternatively, the size of the cubic flexibility window is identical between the filled and empty KFI frameworks. This behaviour mirrors what has been observed previously with the EMT framework,[33] and is similar to the C-form of zeolite RHO herein.

Variation of the unit cell parameters as a function of pressure for the two samples are illustrated in figure 8. For the empty zeolite ZK-5, there is a consistent decline in cell parameter *a* with increasing pressure after the transition into the tetragonal phase. However, in the tetragonal phase there is a sudden contraction in cell parameter *c*, which displays a greater rate of contraction in comparison to the *a* parameter. This demonstrates anisotropic contraction in the tetragonal phase. Furthermore, this suggests that the Daphne oil is no longer transmitting the applied pressure to the zeolite sample hydrostatically.

Similar compression behaviour is observed for the filled zeolite ZK-5 sample, however the initial decline in the *c* parameter with appearance of the tetragonal phase is less prominent. This is expected to be due to the presence of the 18C6 molecule in the α-cage, which prevents such a collapse along the *c* axis. In addition, there is a marginal expansion of cell parameter *a* with the phase transition. For both the empty and filled samples, cell parameter *c* is more compressible than cell parameter *a*. This is anticipated to be due to the decline in symmetry and consequential axial strain in the unit cell.

The tetragonal phase change is shown to be reversible by the return to the ambient cubic symmetry with decompression. For both the empty and filled samples the expansion of the unit cell with decompression mostly follows that of the compression. The exception is with the empty zeolite ZK-5, which shows a hysteresis with the return to the cubic phase. Concerning the filled zeolite ZK-5, due to the lack of datapoints it cannot be explicitly confirmed whether a hysteresis is present or not. However, if a hysteresis is present, the returning cubic phase is still observed at a higher pressure compared to that of the empty sample. We postulate that the steric bulk of the occluded 18C6 molecule aids in the reassertion of the cubic symmetry with declining pressure. This is analogous to the structural memory of zeolites exerted by hydrated cations in the FAU framework,[48,49] as mentioned previously.

Figure 9 displays the unit cell volume contraction as a function of pressure for both samples of zeolite ZK-5, as well as the bulk moduli of the corresponding phases. Due to experimental time constraints, the filled zeolite ZK-5 was depressurised before the onset of pressure-induced amorphisation. In the cubic phase the presence of the 18C6 molecule in the α-cage appears to make the zeolite more compressible. Such behaviour is comparable to that seen for the C-form of zeolite RHO. Consequently, the same rationale can be used, whereby due to the geometric constraints the framework tetrahedra express improved mobility. This further reinforces that there is a geometric congruence between the 18C6 molecule and the α-cage. Moreover, both samples of the cubic phase show a negative pressure derivative, indicative of pressure-induced softening.[46] Previously, Fang and Dove[50] have simulated and predicted such dynamic instabilities for zeolite ZK-5, and other cubic zeolites. However, the pressure derivatives observed herein for zeolite ZK-5 are significantly larger than anticipated.

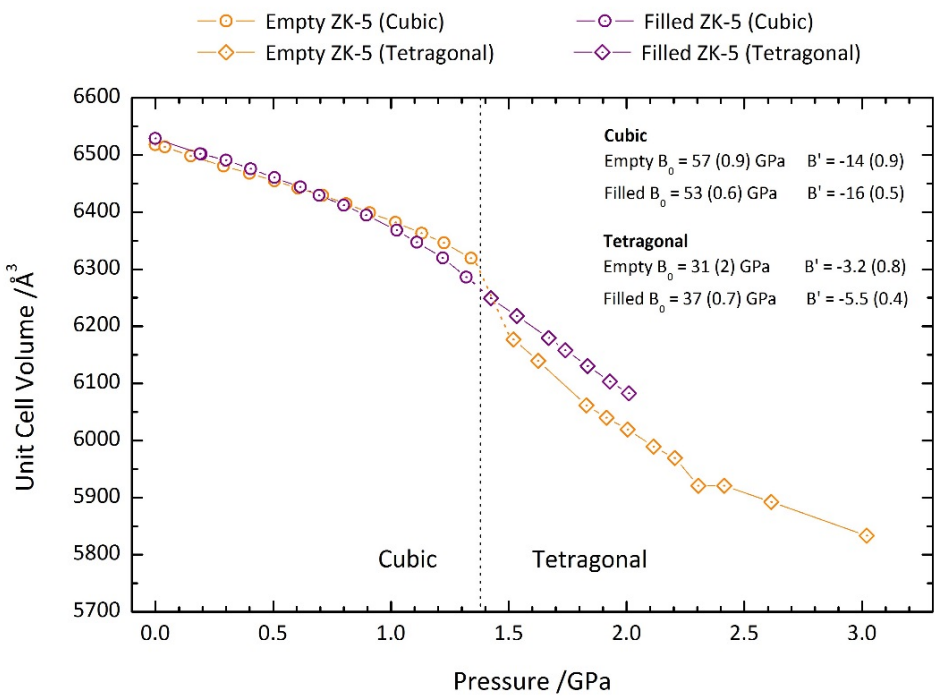

Figure 9. The variation of cell volume with increasing pressure for zeolite ZK-5. The empty analogue is shown in orange, and the filled in purple. Circle data points correspond to the cubic phase, and diamonds to the tetragonal phase. The approximate position of the phase transition is shown with the dotted line. Also included are the bulk moduli (B_0) and pressure derivatives (B') of the two phases of the zeolites, using the Birch-Murnaghan 3rd order fit calculated using the PASCal webtool, as shown in the SI.

With the transition to the tetragonal phase, both the empty and filled zeolite ZK-5 samples show increased compressibility. As with zeolite RHO, this behaviour demonstrates the enhanced compressibility is facilitated by the transition to a lower symmetry. Within the tetragonal phase, the filled zeolite ZK-5 is shown to be less compressible, as is expected. In this case the steric bulk of the 18C6 molecule is preventing the collapse of the framework. This is corroborated by the data itself, which shows how the filled zeolite ZK-5 displays a significantly more expanded unit cell volume than the empty analogue, at the same pressure.

Discussion

From the results herein, it is apparent that zeolites RHO and ZK-5 are comparable with regards to their compression behaviour. As these two zeolites share several symmetry and topological features, this highlights how the compression mechanism is dominated by framework geometry. Specifically, for zeolites RHO and ZK-5, there is the observation that in their ambient symmetries the occlusion of the 18C6 molecule appears to enhance the mechanical softness of the framework. An observation that is further supported by the flexibility windows, which expand or are unchanged with occlusion of 18C6. This contrasts convention, that extra-framework content should reduce the compressibility.[11,25,26]

This behaviour has been rationalised as an influence of geometric constraints imposed by the 18C6 molecule. Such constraints being unique to the α-cage, suggesting an exclusive relationship between the 18C6 molecule and the α-cage geometry. Consequently, the 18C6 molecules expresses behaviour

indicative of a geometric template in the synthesis of zeolites RHO and ZK-5. In contrast, zeolite Na-X shows a contraction of the flexibility window with 18C6 occlusion, but no influence on the mechanical softness due to the 18C6 molecule's own inherent flexibility. This suggests that in the assembly of zeolite Na-X the 18C6 express no specific interactions with the framework, indicative of a space-filling species.

In addition, zeolites RHO and ZK-5 also show a reduction in symmetry with pressure and increase in mechanical softness, which zeolite Na-X does not. Although topologically zeolites RHO and ZK-5 share an α-cage, the reason for this distinction is clearer upon comparison to other cubic and tetragonal zeolites. Table 2 summarises the findings herein alongside the results of other zeolites analysed using high pressure X-ray diffraction in the literature. These results highlight that a phase change with pressure is only observed for zeolites with body-centred symmetry. This is even true when the ambient space group differs between zeolites of the same framework type, as is the case for the ANA-type zeolites.[20-23]

Table 2. A summary of cubic and tetragonal zeolites that have been studied with high pressure X-ray diffraction. Contained are the space groups at ambient conditions and observed under compression.

Zeolite	Framework Type	Ambient Space Group	Pressure-Induced Space Group
Analcime[20]	ANA	$Ia\bar{3}d$	$P\bar{1}$
Leucite[21]	ANA	$I4_1/a$	$P\bar{1}$
Pollucite[22]	ANA	$Ia\bar{3}d$	$P\bar{1}$
Wairakite[23]	ANA	$I2/a$	$P\bar{1}$
Zeolite ZK-5	KFI	$\mathfrak{I}\bar{3}m$	$I4/mmm$
Zeolite Rho[15-17,51]	RHO	$\mathfrak{I}\bar{3}m$	$I\bar{4}3m$
Sodalite[4,52,53]	SOD	$\mathfrak{I}\bar{3}m$	$I\bar{4}3m$
Zeolite A[28,54,55]	LTA	$Fm\bar{3}c$	-
Zeolite Na-X[56]	FAU	$Fd\bar{3}m$	-
Zeolite Y[26]	FAU	$Fd\bar{3}m$	-

We propose, that such pressure-induced symmetry changes are intrinsic of body-centred cubic zeolites. In the ambient form, the zeolite symmetry is so high that the framework is restricted in the degrees of freedom in which the tetrahedra can tilt while maintaining the symmetry. It is geometrically favourable for the symmetry to be lowered, permitting continued compression without compromising the rigid shape of the framework tetrahedra. Consequently, we predict that other body-centred cubic aluminosilicate zeolites will also express pressure-induced symmetry changes upon compression. Paulingite being a candidate zeolite. Furthermore, we also anticipate that other aluminosilicate zeolites, such as tschörtnerite and Linde Type N, will show no such change in symmetry.

Conclusion

High pressure powder X-ray diffraction data demonstrates a pressure-induced symmetry change from cubic to tetragonal for zeolite ZK-5. For zeolites RHO and ZK-5, the presence of 18C6 within the framework cavities does not influence the pressure at which symmetry transitions occur. In both

cases, the 18C6 containing zeolite is more compressible than the empty framework, suggesting geometric match-up with the α-cage. For zeolite Na-X, the 18C6 molecule expresses negligible influence on the mechanical softness of the framework. From observing the influence of the 18C6 molecule on framework dynamics, it is discerned that 18C6 behaves as a space-filling species in the preparation of zeolite Na-X and employs geometric structure direction for zeolites RHO and ZK-5.

In conjunction with previous high pressure analysis in the literature, we propose that pressure-induced reductions in symmetry are intrinsic to body-centred cubic zeolites. The phase transition is geometrically driven and allows the framework to be compressed further without distorting the framework tetrahedra, which is energetically costly.

Acknowledgements

A.S. thanks the Royal Society for funding. Both A.N. and P.R.R. thank the EPSRC for funding (EP/K004956/1). The high pressure X-ray diffraction data herein was collected on beamline ID15B at the European Synchrotron Radiation Facility (ESRF), Grenoble, France. We thank the ESRF Council for accepting our research proposal. We are also grateful to I.E.C at the ESRF for assisting with the data collection.

Author Contributions

The original manuscript was written and prepared by A.N. with input from all co-authors. Sample preparation was performed by A.N. The geometric simulations in GASP were performed by M.U.C. Pawley refinements using TOPAS Academic were performed by A.N. The experimental high pressure X-ray diffraction data was obtained using the ID15B beamline at the ESRF, collected by A.N., M.U.C., Z.L.J. and A.S. who were assisted by I.E.C. All authors were involved in the data interpretation and editing of the manuscript.

Data Availability

All data creating during this study is available free of charge from the University of Bath data archive at [URL to be added on acceptance.].

Supplementary Information

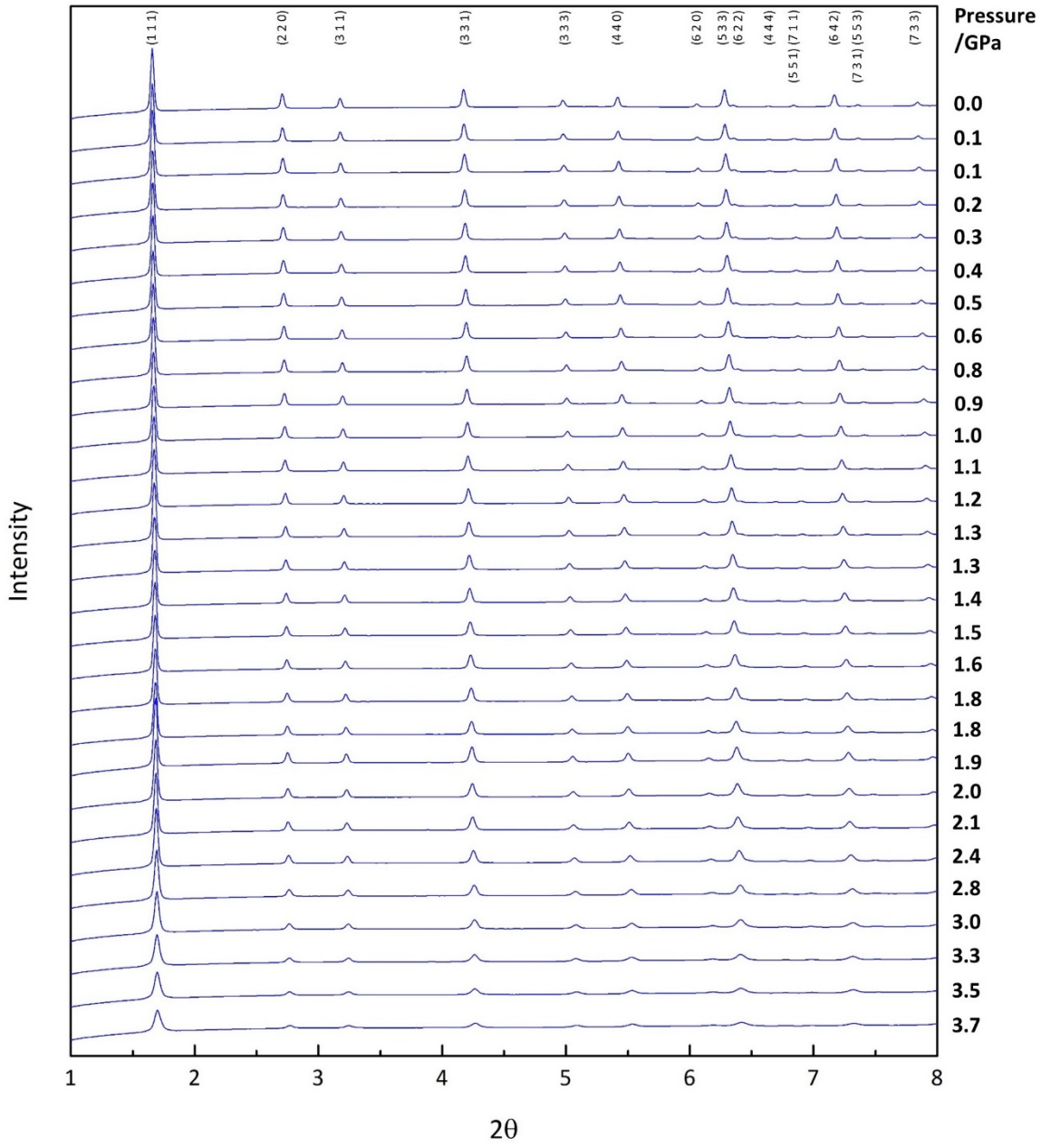

Figure S1. Powder X-ray diffraction patterns (2θ = 1-8°) of empty zeolite Na-X (FAU) as a function of pressure throughout the compression cycle.

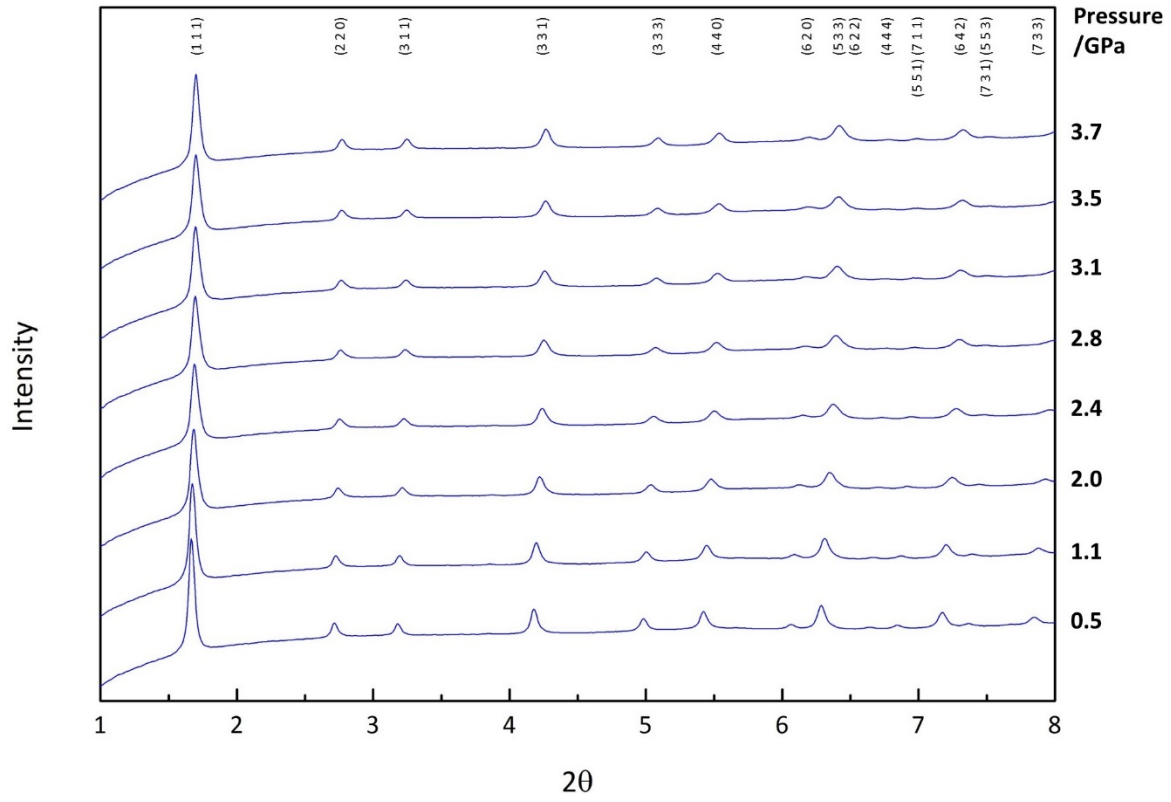

Figure S2. Powder X-ray diffraction patterns (2θ = 1-8°) of empty zeolite Na-X (FAU) as a function of pressure throughout the decompression cycle.

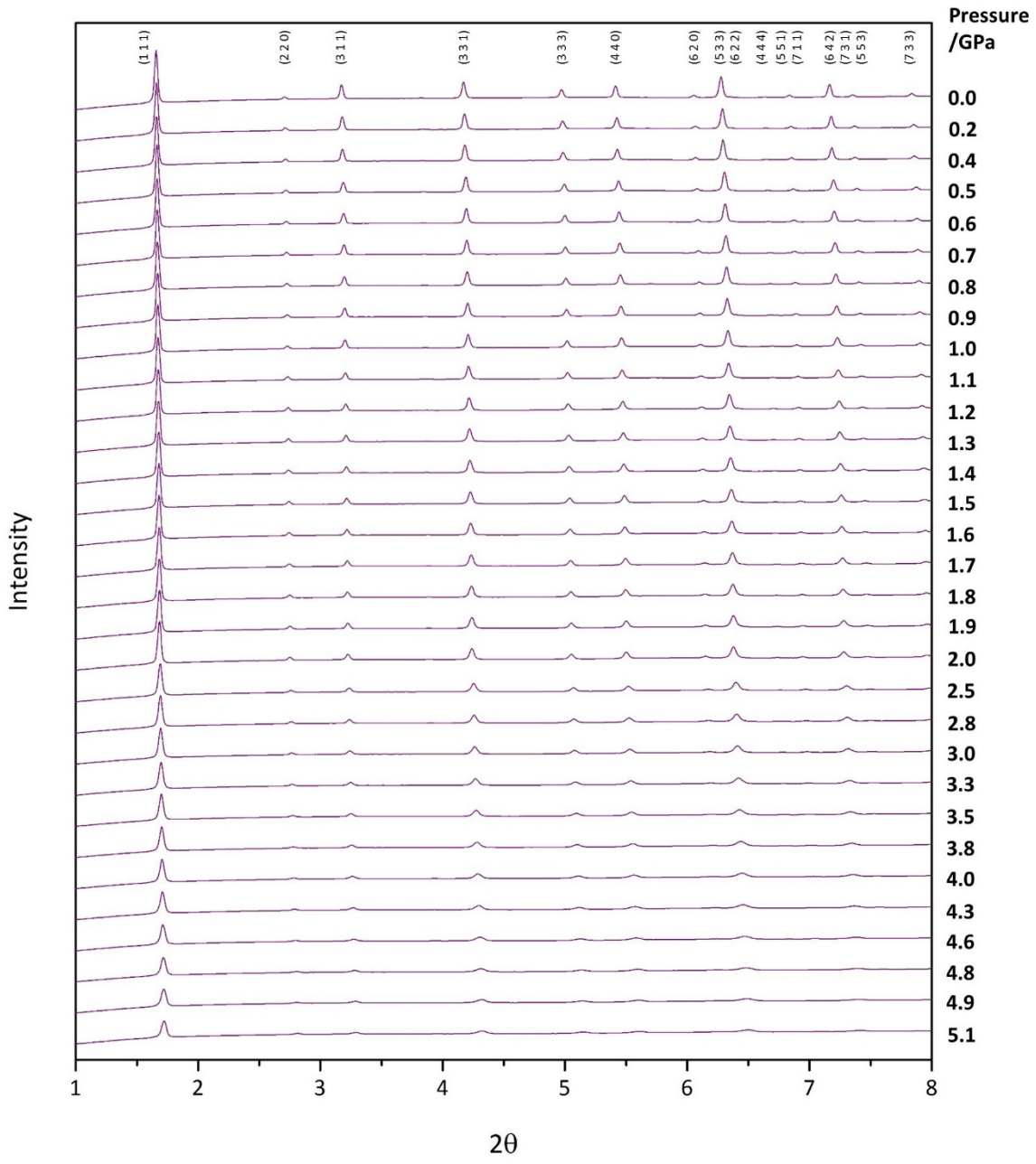

Figure S3. Powder X-ray diffraction patterns (2θ = 1-8°) of filled zeolite Na-X (FAU) as a function of pressure throughout the compression cycle.

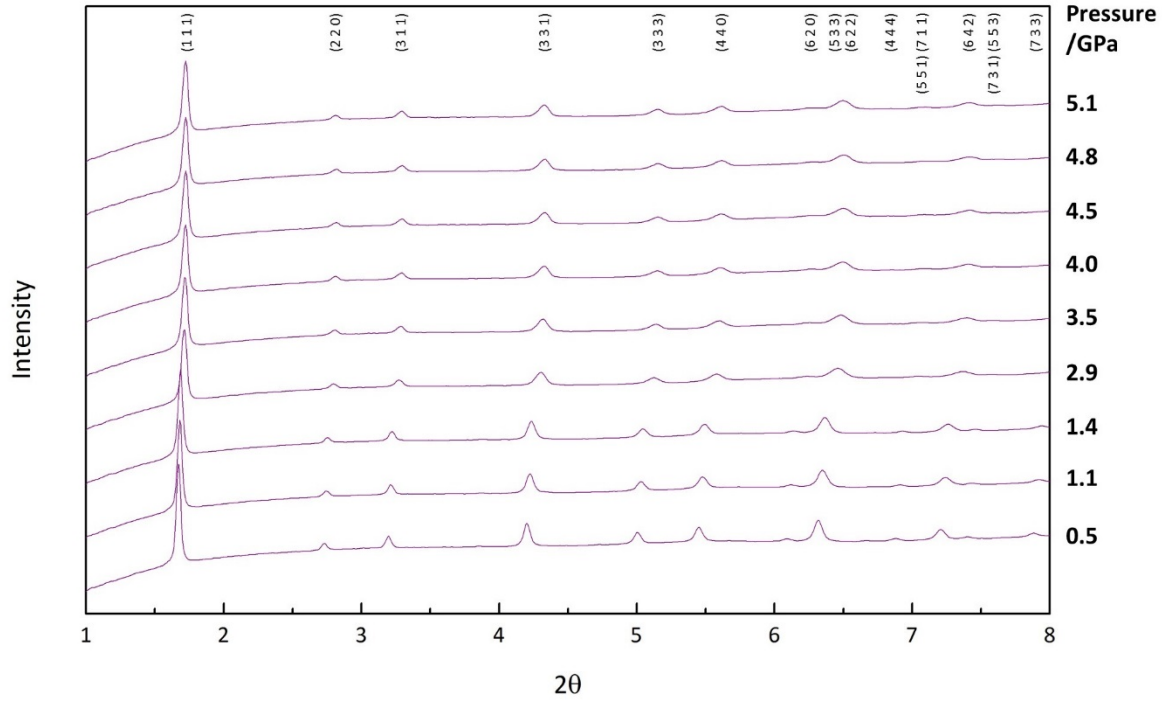

Figure S4. Powder X-ray diffraction patterns (2θ = 1-8°) of filled zeolite Na-X (FAU) as a function of pressure throughout the decompression cycle.

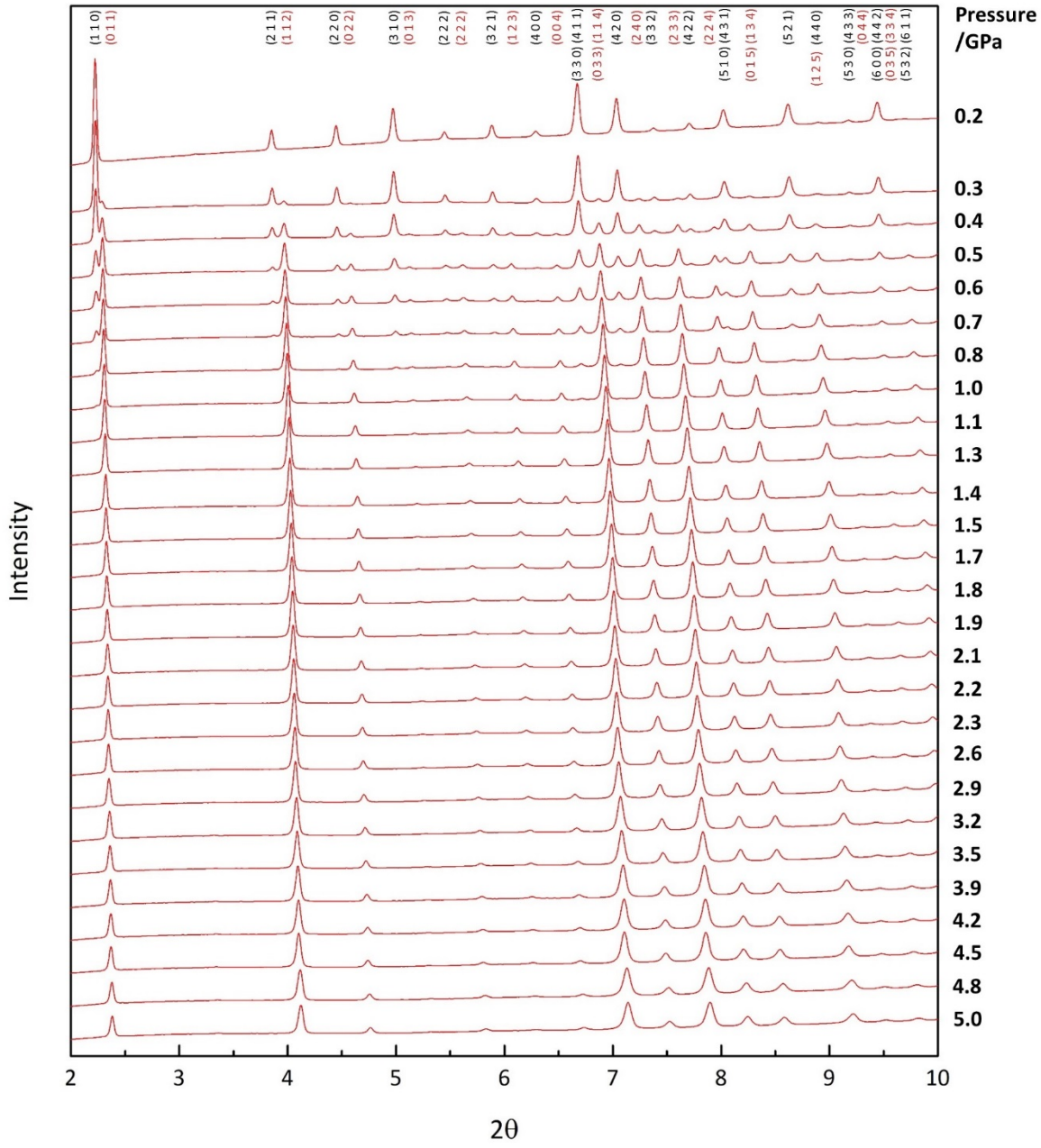

Figure S5. Powder X-ray diffraction patterns (2θ = 2-10°) of empty zeolite RHO (RHO) as a function of pressure throughout the compression cycle. Miller indices corresponding to the C-form are shown in black, and the A-form in red.

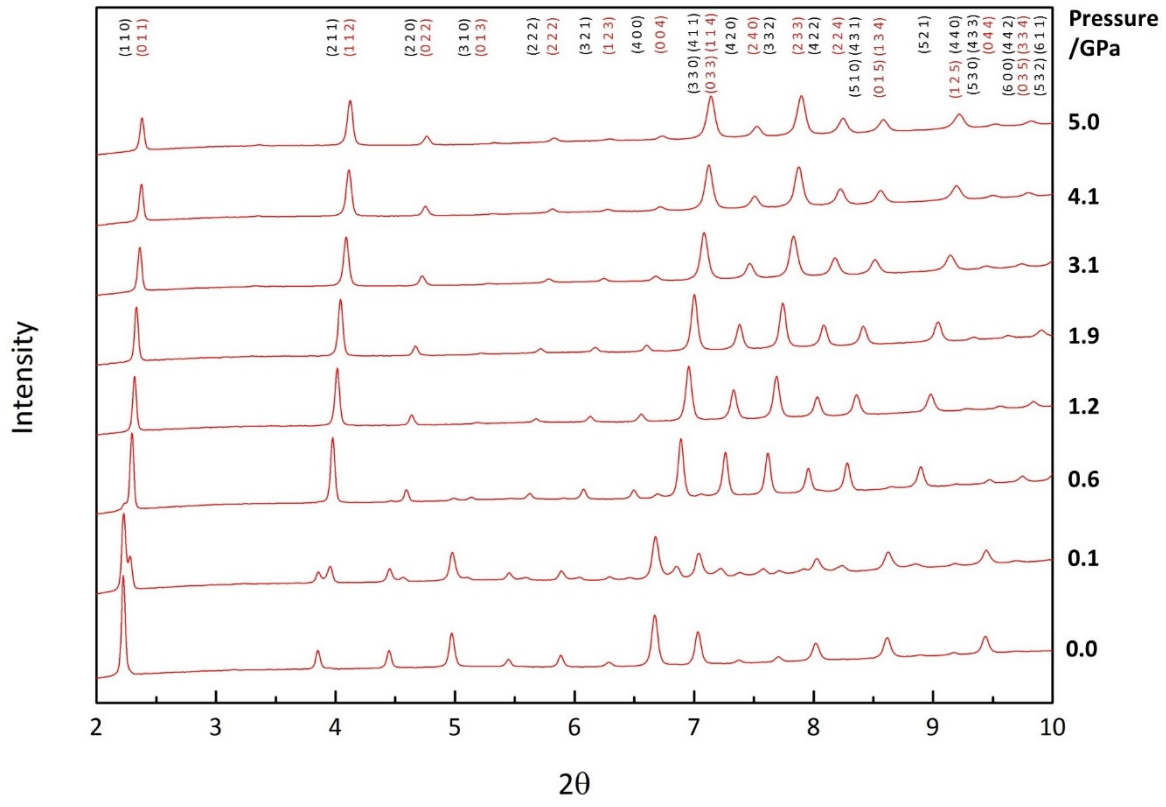

Figure S6. Powder X-ray diffraction patterns (2θ = 2-10°) of empty zeolite RHO (RHO) as a function of pressure throughout the decompression cycle. Miller indices corresponding to the C-form are shown in black, and the A-form in red.

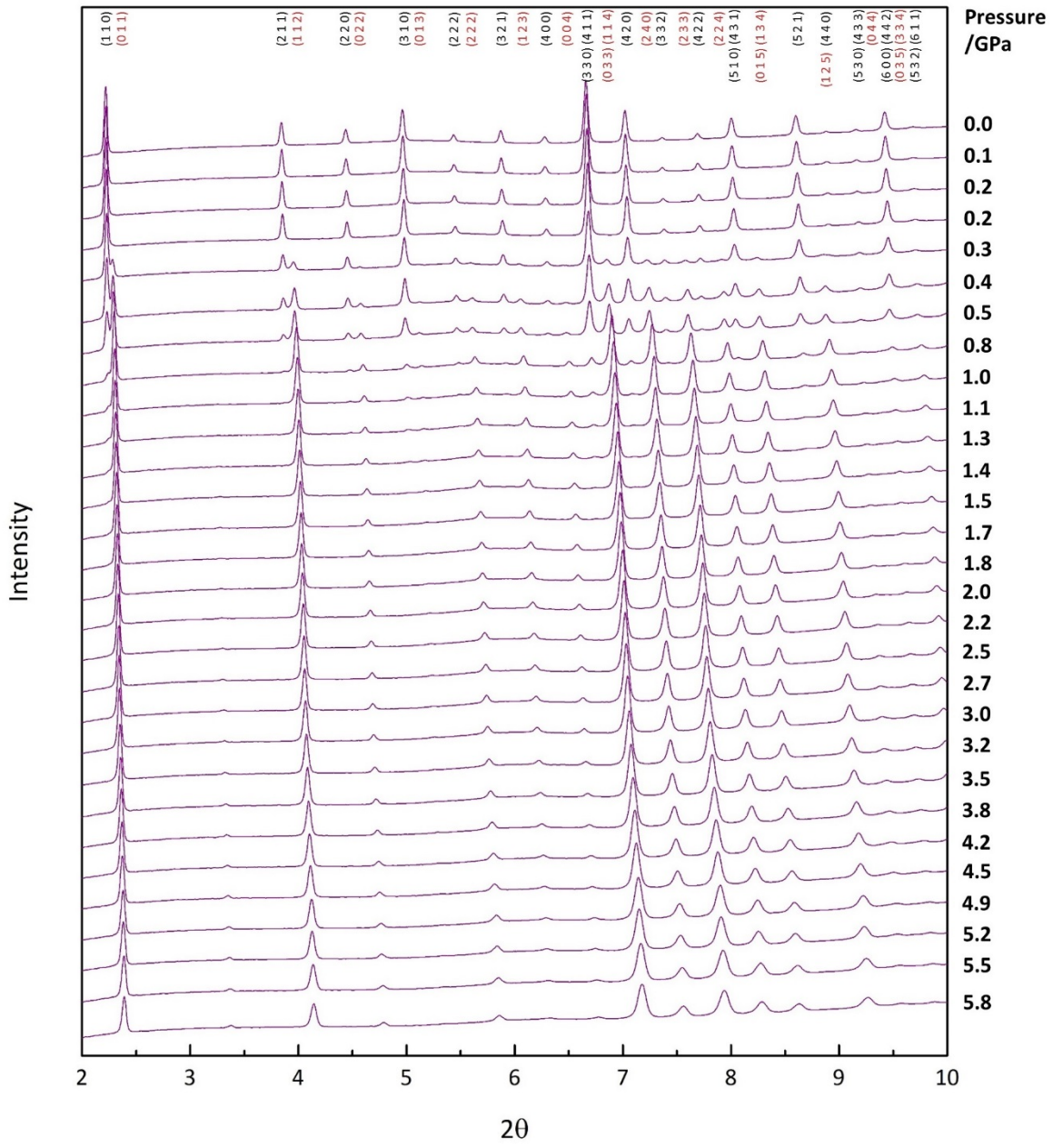

Figure S7. Powder X-ray diffraction patterns (2θ = 2-10°) of filled zeolite RHO (RHO) as a function of pressure throughout the compression cycle. Miller indices corresponding to the C-form are shown in black, and the A-form in red.

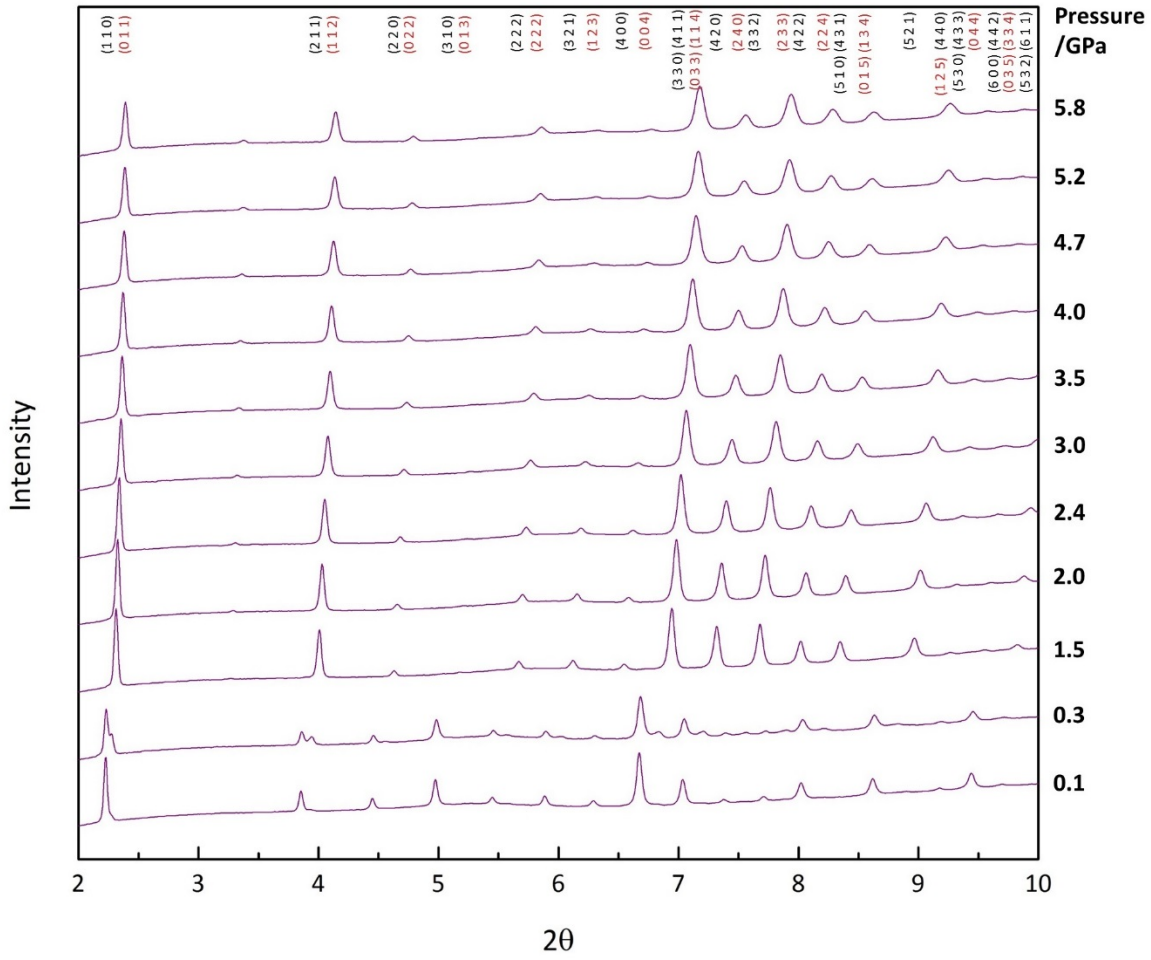

Figure S8. Powder X-ray diffraction patterns (2θ = 2-10°) of filled zeolite RHO (RHO) as a function of pressure throughout the decompression cycle. Miller indices corresponding to the C-form are shown in black, and the A-form in red.

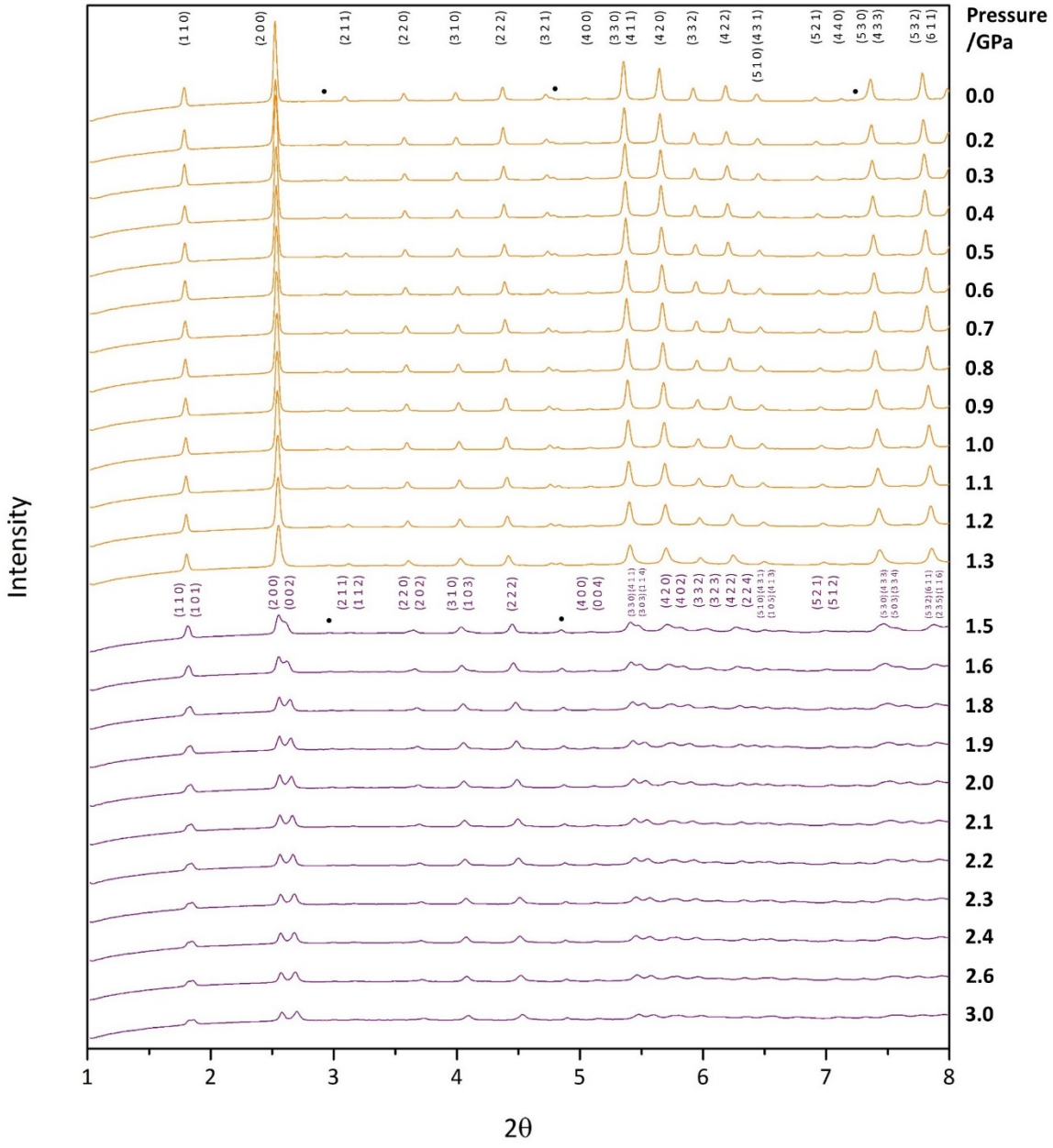

Figure S9. Powder X-ray diffraction patterns (2θ = 1-8°) of empty zeolite ZK-5 (KFI) as a function of pressure throughout the compression cycle. Patterns identified as the cubic form are shown in orange, and the tetragonal form in purple. Miller indices corresponding to the cubic form are shown in black, and the tetragonal form in purple. The dot refers to Bragg peaks from the zeolite W (MER) impurity phase.

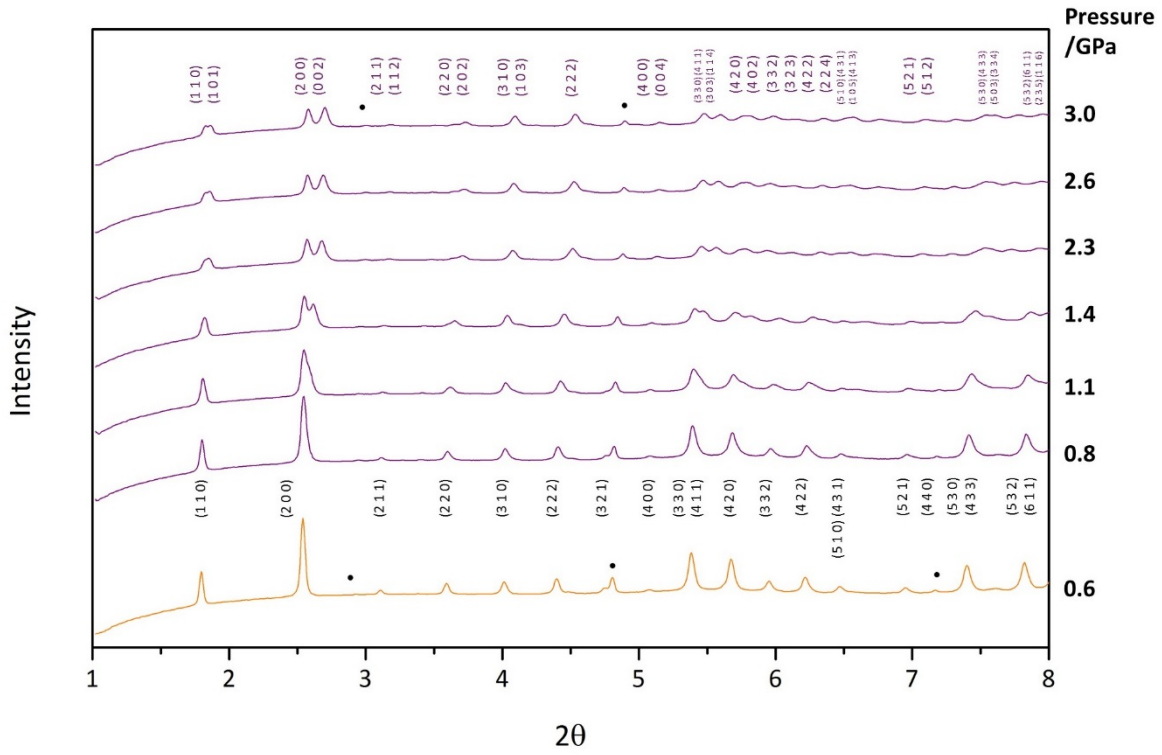

Figure S10. Powder X-ray diffraction patterns (2θ = 1-8°) of empty zeolite ZK-5 (KFI) as a function of pressure throughout the decompression cycle. Patterns identified as the cubic form are shown in orange, and the tetragonal form in purple. Miller indices corresponding to the cubic form are shown in black, and the tetragonal form in purple. The dot refers to Bragg peaks from the zeolite W (MER) impurity phase.

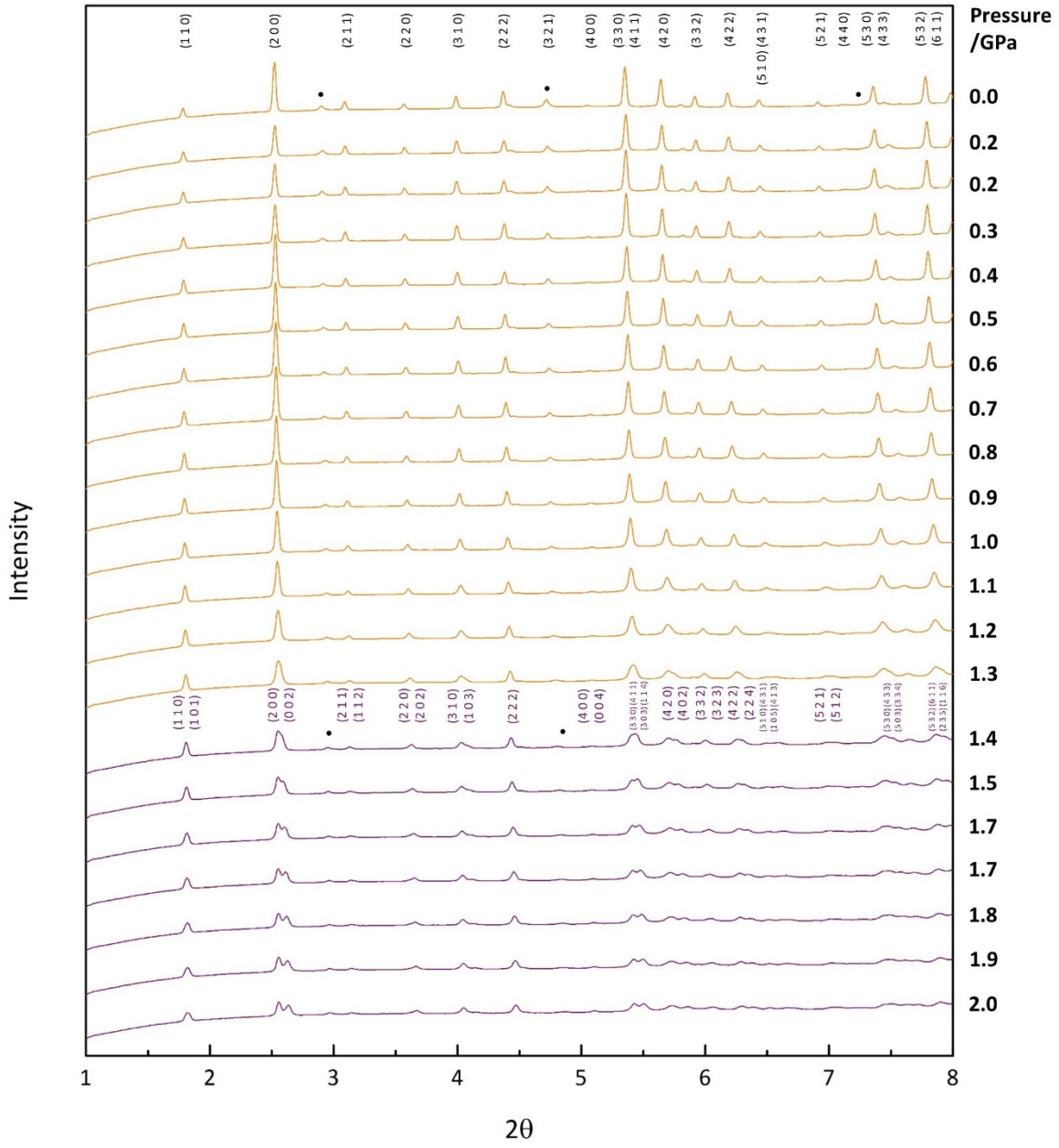

Figure S11. Powder X-ray diffraction patterns (2θ = 1-8°) of filled zeolite ZK-5 (KFI) as a function of pressure throughout the compression cycle. Patterns identified as the cubic form are shown in orange, and the tetragonal form in purple. Miller indices corresponding to the cubic form are shown in black, and the tetragonal form in purple. The dot refers to Bragg peaks from the zeolite W (MER) impurity phase.

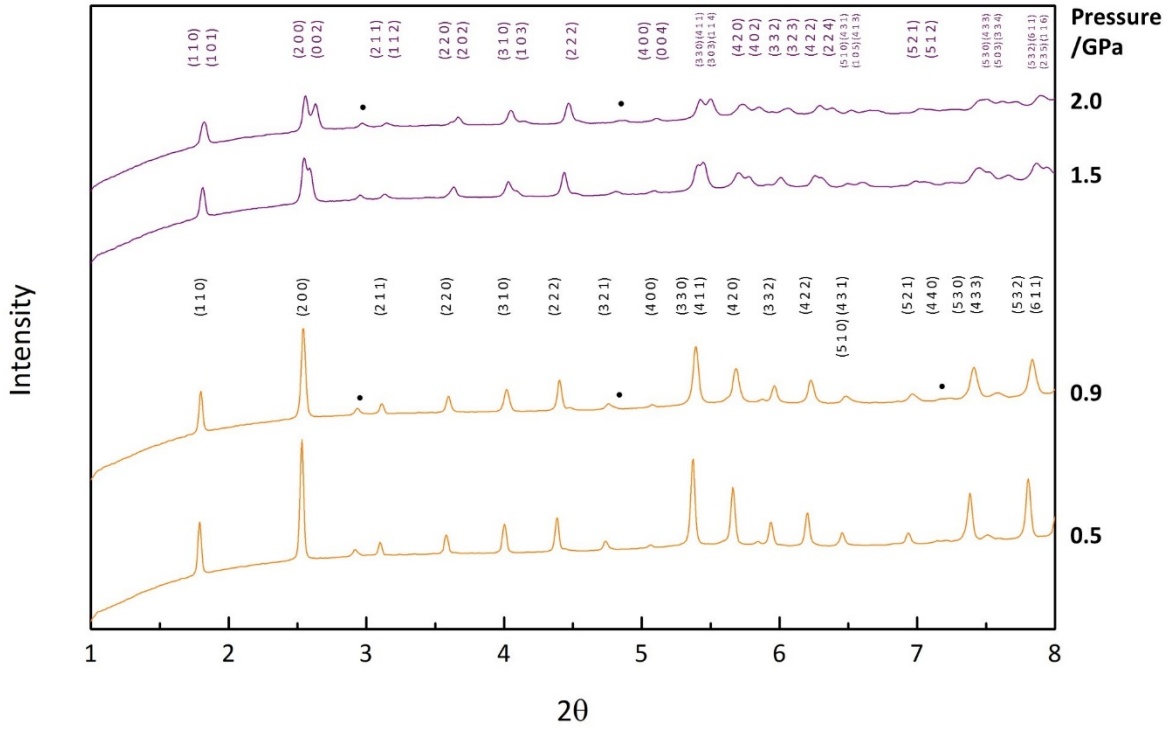

Figure S12. Powder X-ray diffraction patterns (2θ = 1-8°) of filled zeolite ZK-5 (KFI) as a function of pressure throughout the decompression cycle. Patterns identified as the cubic form are shown in orange, and the tetragonal form in purple. Miller indices corresponding to the cubic form are shown in black, and the tetragonal form in purple. The dot refers to Bragg peaks from the zeolite W (MER) impurity phase.

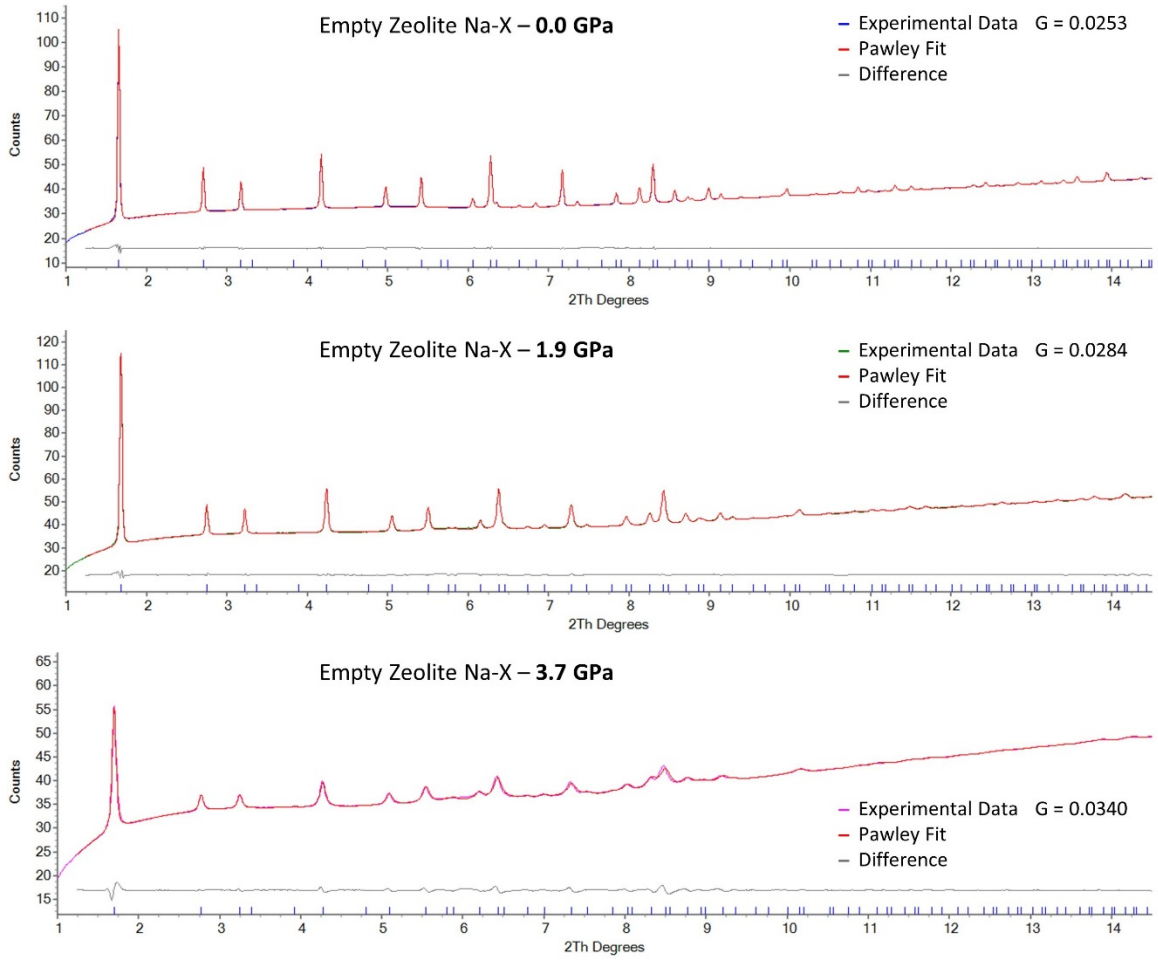

Figure S13. Final refined Pawley fits for empty zeolite Na-X (FAU) at pressures of 0.0, 1.9 and 3.7 GPa. The patterns in blue, green and pink correspond to the experimental data, red to the Pawley fit and grey to the difference. G refers to the 'goodness of fit'.

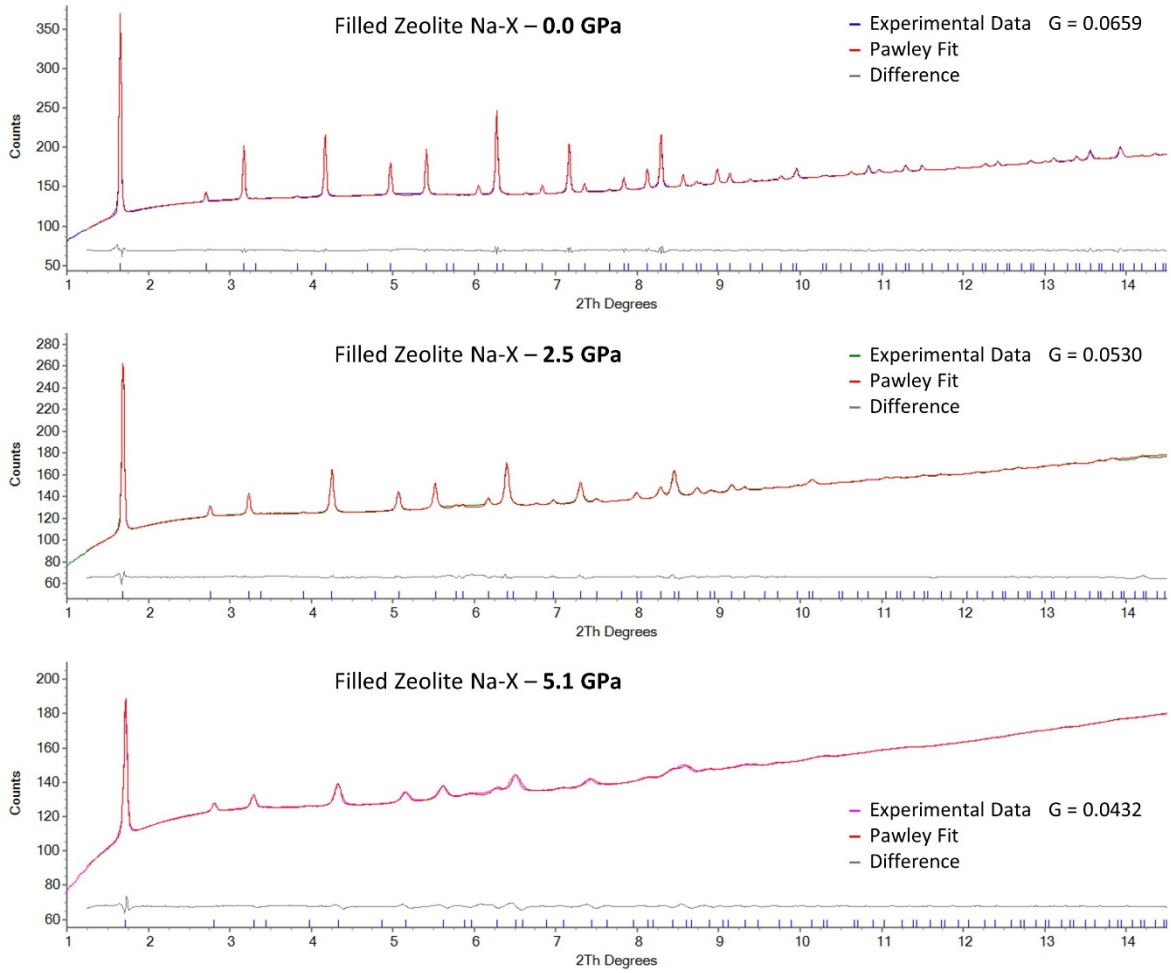

Figure S14. Final refined Pawley fits for filled zeolite Na-X (FAU) at pressures of 0.0, 2.5 and 5.1 GPa. The patterns in blue, green and pink correspond to the experimental data, red to the Pawley fit and grey to the difference. G refers to the 'goodness of fit'.

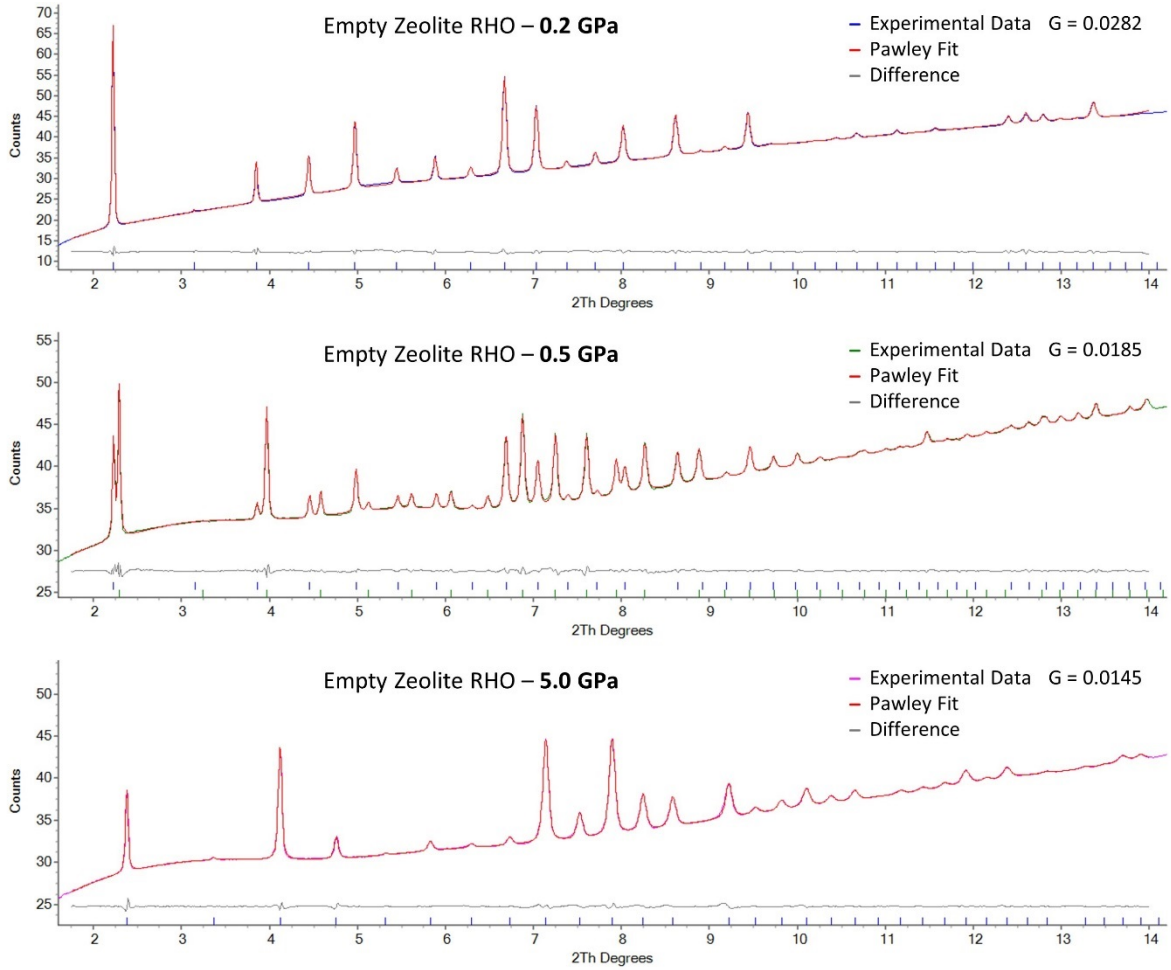

Figure S15. Final refined Pawley fits for empty zeolite RHO (RHO) at pressures of 0.2, 0.5 and 5.0 GPa. At 0.2 GPa only the C-form is present, at 0.5 GPa both forms are present and at 5.0 GPa only the A-form is present. The patterns in blue, green and pink correspond to the experimental data, red to the Pawley fit and grey to the difference. G refers to the 'goodness of fit'.

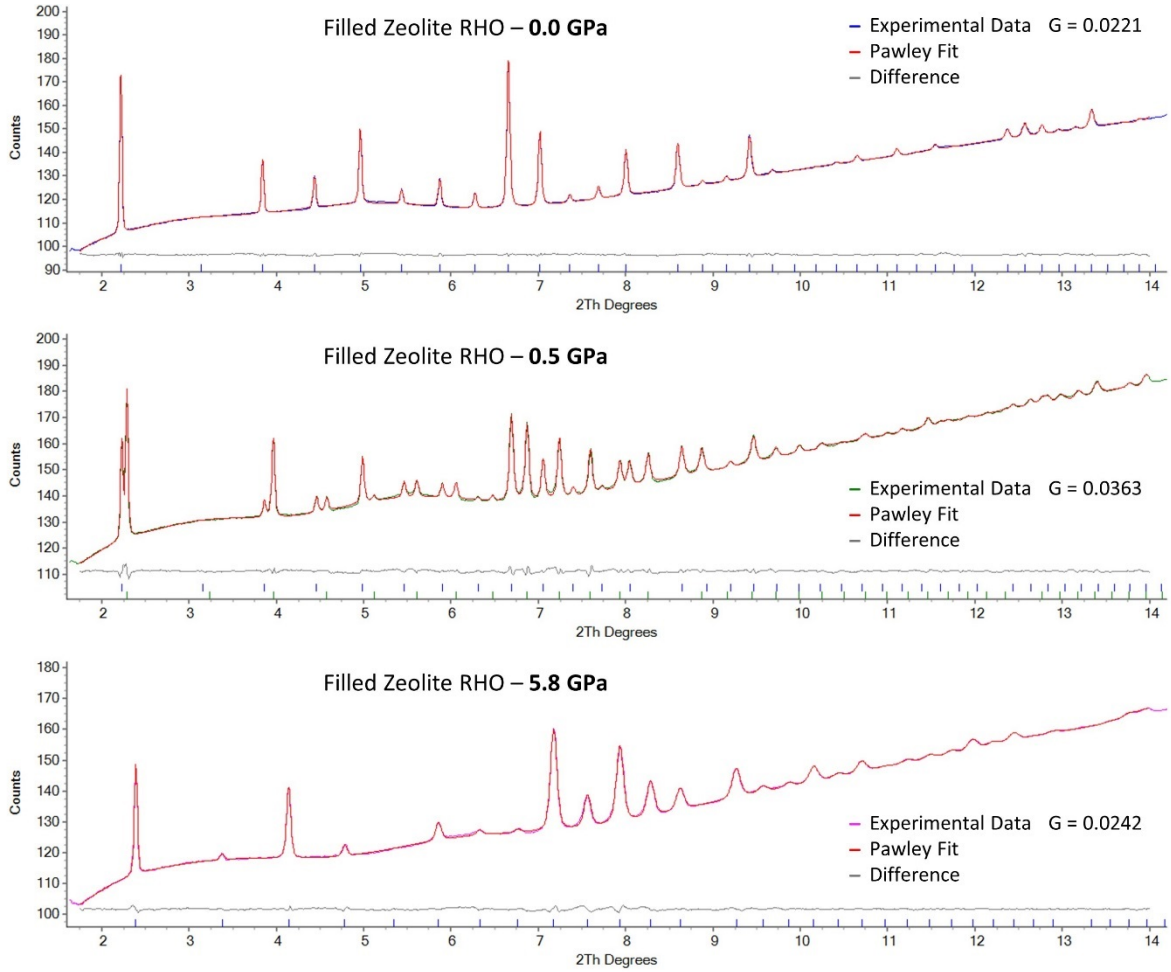

Figure S16. Final refined Pawley fits for filled zeolite RHO (RHO) at pressures of 0.0, 0.5 and 5.8 GPa. At 0.0 GPa only the C-form is present, at 0.5 GPa both forms are present and at 5.8 GPa only the A-form is present. The patterns in blue, green and pink correspond to the experimental data, red to the Pawley fit and grey to the difference. G refers to the 'goodness of fit'.

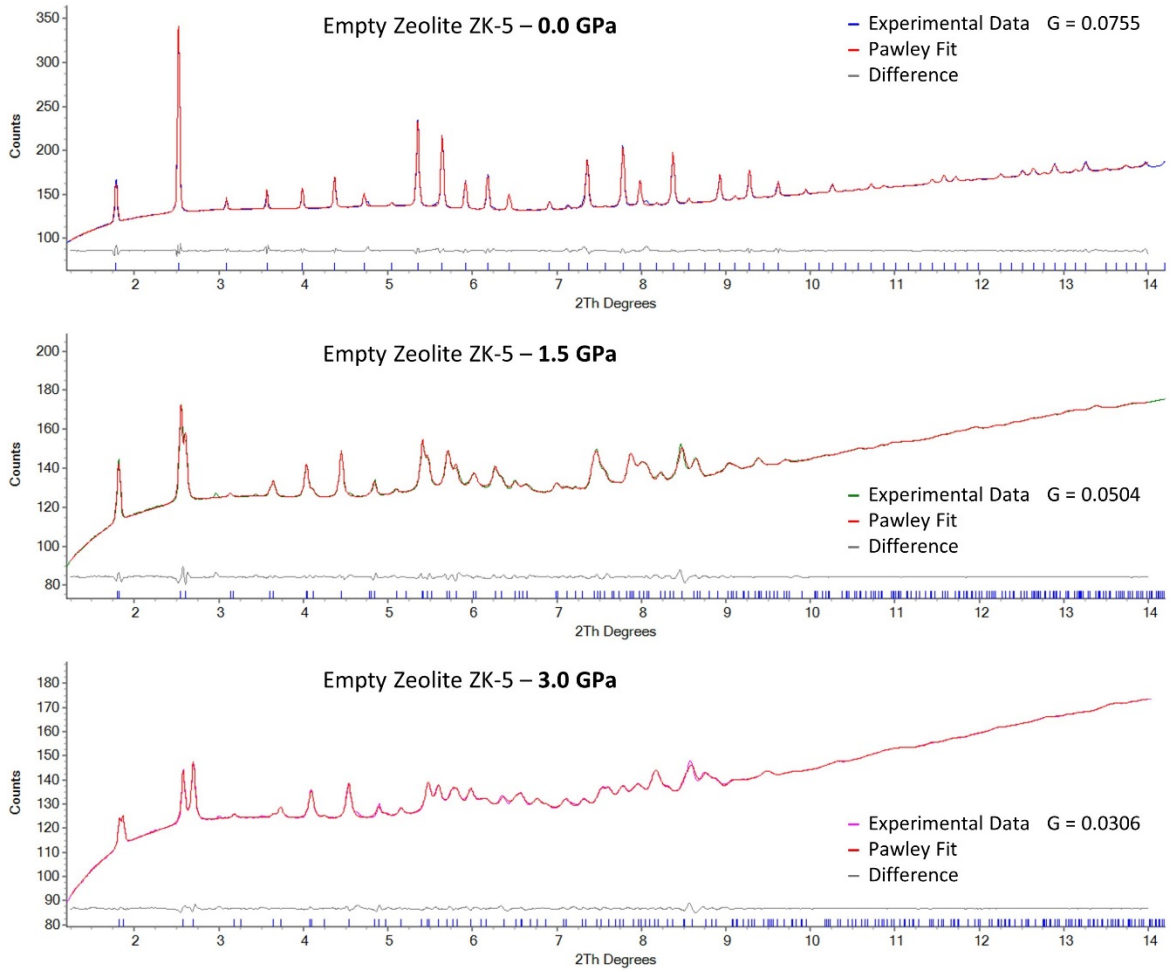

Figure S17. Final refined Pawley fits for empty zeolite ZK-5 (KFI) at pressures of 0.0, 1.5 and 3.0 GPa. At 0.0 GPa the zeolite is in the cubic phase, and at 1.5 and 3.0 GPa it is in the tetragonal phase. The patterns in blue, green and pink correspond to the experimental data, red to the Pawley fit and grey to the difference. G refers to the 'goodness of fit'.

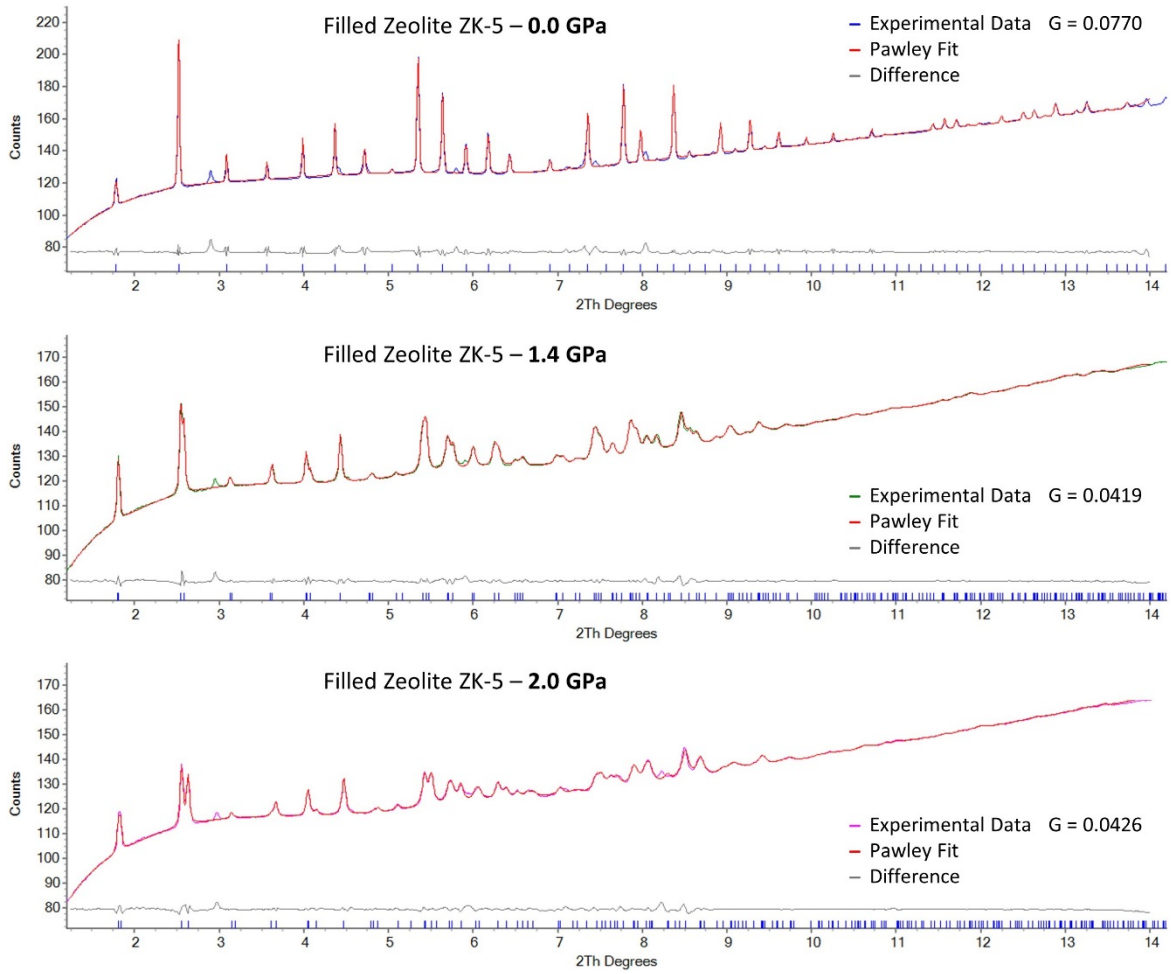

Figure S18. Final refined Pawley fits for filled zeolite ZK-5 (KFI) at pressures of 0.0, 1.4 and 2.0 GPa. At 0.0 GPa the zeolite is in the cubic phase, and at 1.4 and 2.0 GPa it is in the tetragonal phase. The patterns in blue, green and pink correspond to the experimental data, red to the Pawley fit and grey to the difference. G refers to the 'goodness of fit'.

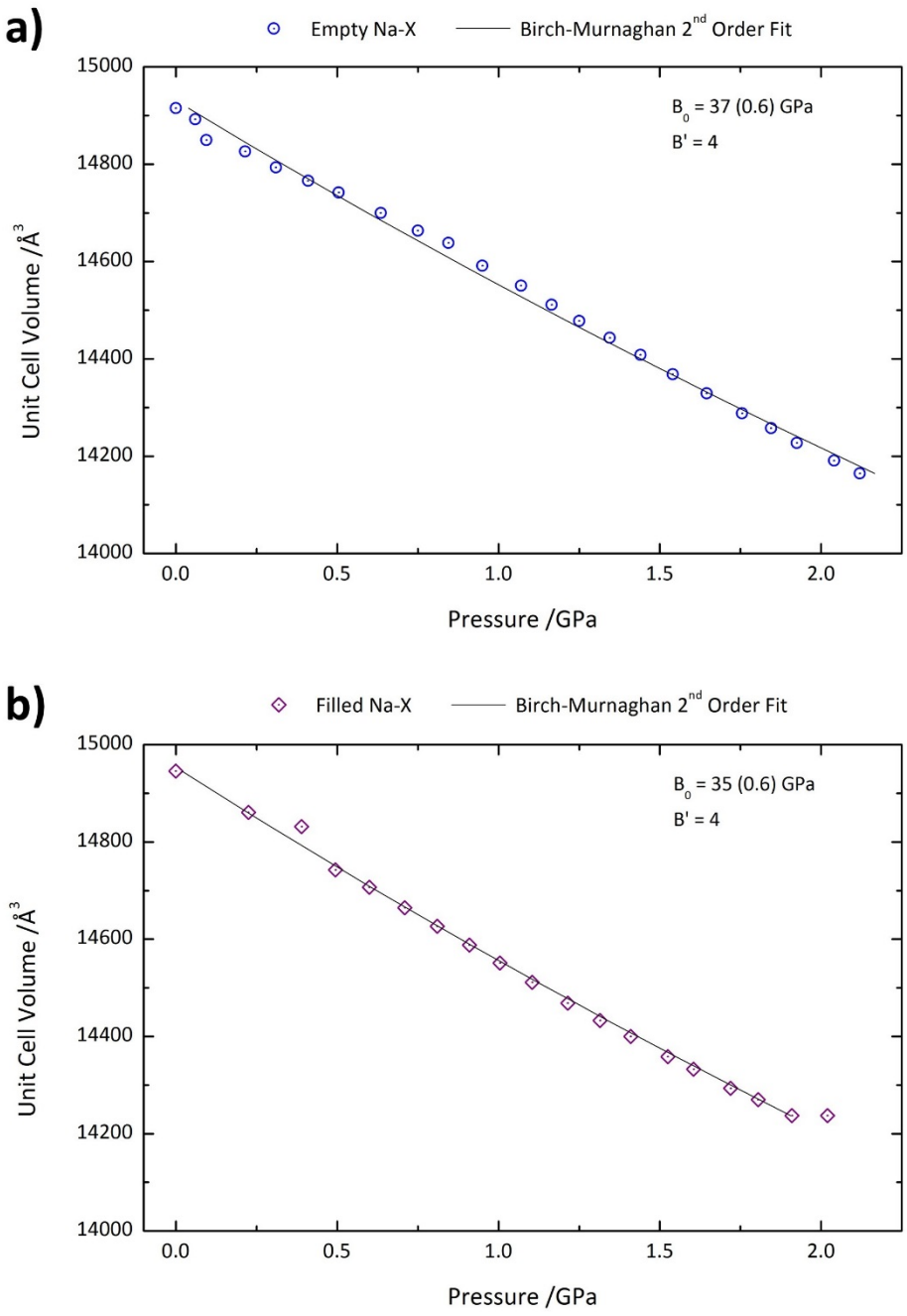

Figure S19. The variation in unit cell volume with pressure for a) the empty and b) the filled zeolite Na-X samples, in the 0-2.2 GPa pressure range. Shown are the Birch-Murnaghan 2nd order fits, bulk moduli (B_0) and pressure derivatives (B') determined using the webtool PASCal.[46]

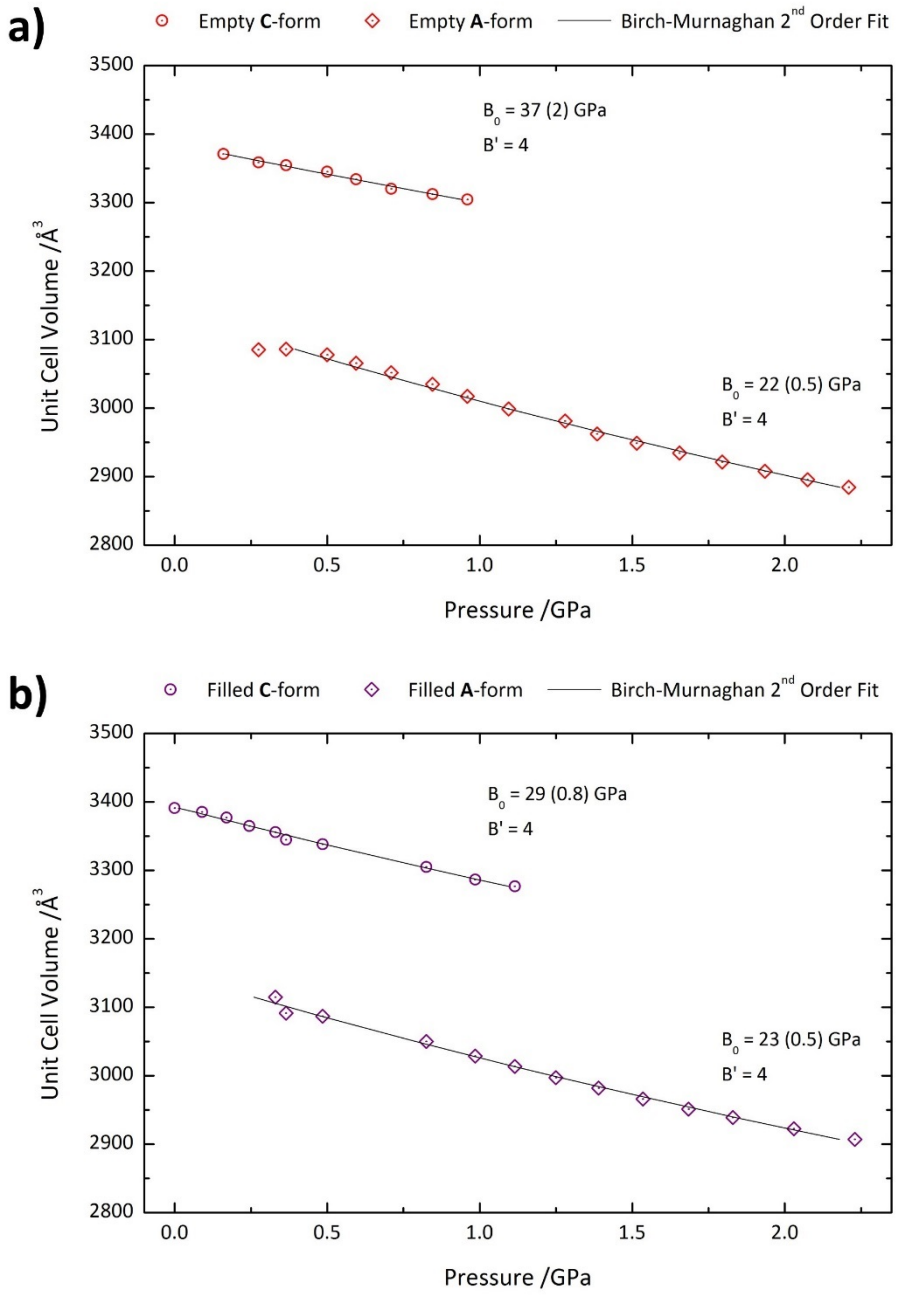

Figure S20. The variation in unit cell volume with pressure for a) the empty and b) the filled zeolite RHO samples, in the 0-2.2 GPa pressure range. Shown are the Birch-Murnaghan 2nd order fits, bulk moduli (B_0) and pressure derivatives (B') determined using the webtool PASCal[46] for both the C and A-forms observed. The C-form is shown with circle data points, and the A-form with diamonds.

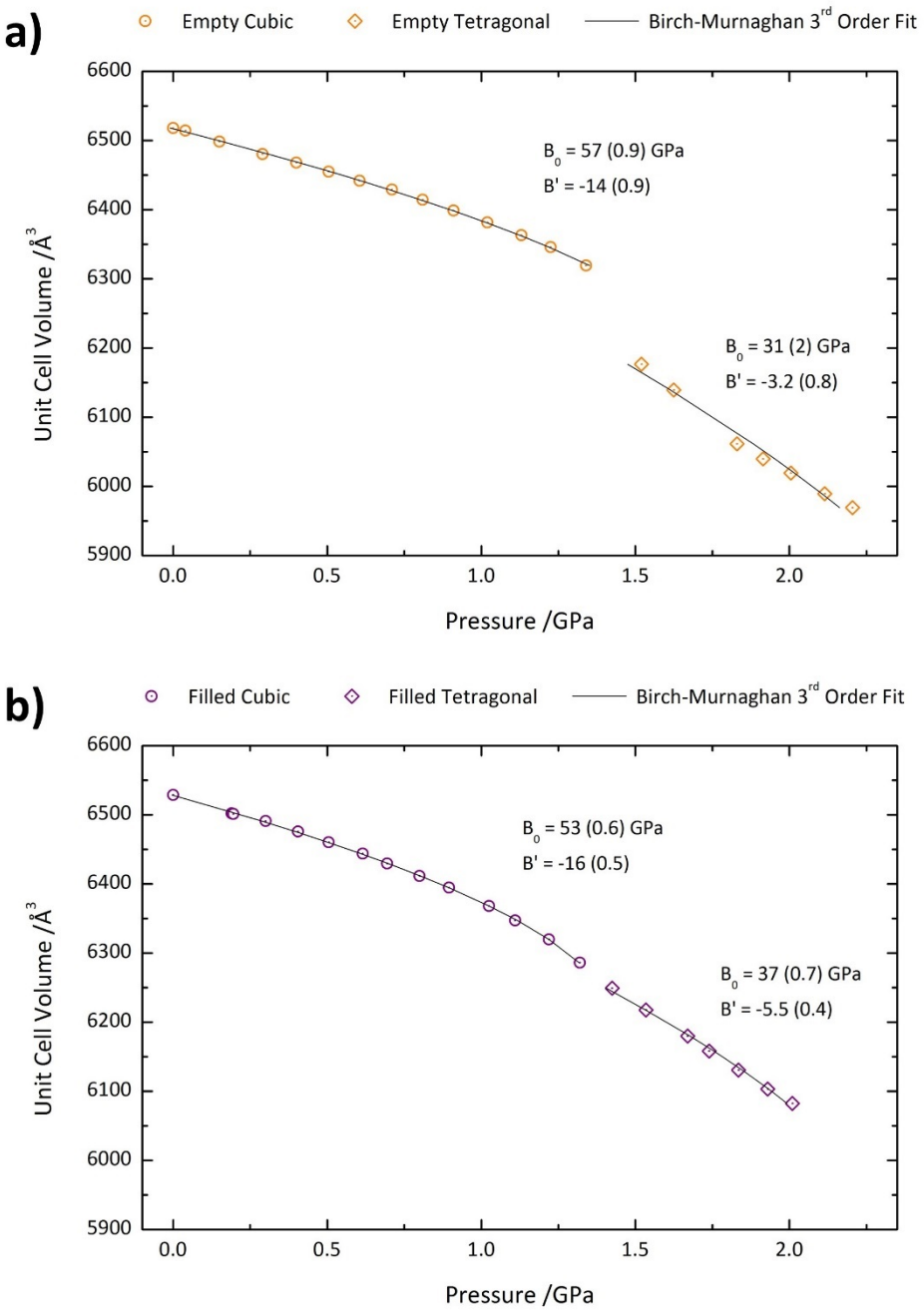

Figure S21. The variation in unit cell volume with pressure for a) the empty and b) the filled zeolite ZK-5 samples, in the 0-2.2 GPa pressure range. Shown are the Birch-Murnaghan 3rd order fits, bulk moduli (B_0) and pressure derivatives (B') determined using the webtool PASCal[46] for both the cubic and tetragonal phases observed. The cubic phase is shown with circle data points, and the tetragonal phase with diamonds.

Bibliography

1 Barrer, R. M. *Hydrothermal Chemistry of Zeolites*. United States Edition edn, (Academic Press Inc. Ltd., 1982).

2 Breck, D. W. *Zeolite molecular sieves: structure, chemistry and use*. (Krieger, 1984).

3 Sartbaeva, A., Wells, S. A., Treacy, M. & Thorpe, M. The flexibility window in zeolites. *Nature materials* **5**, 962 (2006).

4 Kapko, V., Dawson, C., Treacy, M. & Thorpe, M. Flexibility of ideal zeolite frameworks. *Physical Chemistry Chemical Physics* **12**, 8531-8541 (2010).

5 Sartbaeva, A. & Wells, S. A. Framework flexibility and rational design of new zeolites for catalysis. *Applied Petrochemical Research* **2**, 69-72 (2012).

6 Dawson, C. J., Kapko, V., Thorpe, M. F., Foster, M. D. & Treacy, M. M. Flexibility as an indicator of feasibility of zeolite frameworks. *The Journal of Physical Chemistry C* **116**, 16175-16181 (2012).

7 Dove, M. T., Giddy, A. P. & Heine, V. Rigid unit mode model of displacive phase transitions in framework silicates. *Transactions of the American Crystallographic Association* **27**, 65-75 (1993).

8 Lee, Y. *et al.* New insight into cation relocations within the pores of zeolite rho: In situ synchrotron X-ray and neutron powder diffraction studies of Pb-and Cd-exchanged rho. *The Journal of Physical Chemistry B* **105**, 7188-7199 (2001).

9 Gatta, G. D. A comparative study of fibrous zeolites under pressure. *European Journal of Mineralogy* **17**, 411-421 (2005).

10 Gatta, G. D. Does porous mean soft? On the elastic behaviour and structural evolution of zeolites under pressure. *Zeitschrift für Kristallographie-Crystalline Materials* **223**, 160-170 (2008).

11 Wells, S. A., Leung, K. M., Edwards, P. P., Tucker, M. G. & Sartbaeva, A. Defining the flexibility window in ordered aluminosilicate zeolites. *Royal Society open science* **4**, 170757 (2017).

12 Sartbaeva, A., Gatta, G. D. & Wells, S. A. Flexibility window controls pressure-induced phase transition in analcime. *Epl* **83**, doi:10.1209/0295-5075/83/26002 (2008).

13 Sartbaeva, A. *et al.* Flexibility windows and compression of monoclinic and orthorhombic silicalites. *Physical Review B* **85**, 064109 (2012).

14 Jorda, J. L. *et al.* Synthesis of a Novel Zeolite through a Pressure-Induced Reconstructive Phase Transition Process. *Angewandte Chemie-International Edition* **52**, 10458-10462, doi:10.1002/anie.201305230 (2013).

15 Lee, Y., Vogt, T., Hriljac, J. A. & Parise, J. B. Discovery of a rhombohedral form of the Li-exchanged aluminogermanate zeolite RHO and its pressure-, temperature-, and composition-induced phase transitions. *Chemistry of Materials* **14**, 3501-3508, doi:10.1021/cm020257r (2002).

16 Lee, Y. *et al.* Phase transition of zeolite RHO at high-pressure. *Journal of the American Chemical Society* **123**, 8418-8419, doi:10.1021/ja0161554 (2001).

17 Corbin, D. R. *et al.* Flexibility of the zeolite rho framework: in situ X-ray and neutron powder structural characterization of divalent cation-exchanged zeolite rho. *Journal of the American Chemical Society* **112**, 4821-4830 (1990).

18 Parise, J. B. *et al.* Flexibility of the framework of zeolite Rho. Structural variation from 11 to 573 K. A study using neutron powder diffraction data. *The Journal of Physical Chemistry* **88**, 2303-2307 (1984).

19 Palomino, M., Corma, A., Jorda, J. L., Rey, F. & Valencia, S. Zeolite Rho: a highly selective adsorbent for CO 2/CH 4 separation induced by a structural phase modification. *Chemical Communications* **48**, 215-217 (2012).

20 Gatta, G. D., Nestola, F. & Ballaran, T. B. Elastic behavior, phase transition, and pressure induced structural evolution of analcime. *American Mineralogist* **91**, 568-578, doi:10.2138/am.2006.1994 (2006).

21 Gatta, G. D., Rotiroti, N., Ballaran, T. B. & Pavese, A. Leucite at high pressure: Elastic behavior, phase stability, and petrological implications. *American Mineralogist* **93**, 1588-1596, doi:10.2138/am.2008.2932 (2008).
22 Gatta, G. D., Rotiroti, N., Ballaran, T. B., Sanchez-Valle, C. & Pavese, A. Elastic behavior and phase stability of pollucite, a potential host for nuclear waste. *American Mineralogist* **94**, 1137-1143, doi:10.2138/am.2009.3195 (2009).
23 Ori, S., Quartieri, S., Vezzalini, G. & Dmitriev, V. Pressure-induced structural deformation and elastic behavior of wairakite. *American Mineralogist* **93**, 53-62, doi:10.2138/am.2008.2554 (2008).
24 Wells, S., Sartbaeva, A. & Gatta, G. Flexibility windows and phase transitions of ordered and disordered ANA framework zeolites. *EPL (Europhysics Letters)* **94**, 56001 (2011).
25 Gatta, G. & Lee, Y. Zeolites at high pressure: A review. *Mineralogical Magazine* **78**, 267-291 (2014).
26 Colligan, M. *et al.* Synchrotron X-ray powder diffraction and computational investigation of purely siliceous zeolite Y under pressure. *Journal of the American Chemical Society* **126**, 12015-12022, doi:10.1021/ja048685g (2004).
27 Hazen, R. & Finger, L. Compressibility of zeolite 4A is dependent on the molecular size of the hydrostatic pressure medium. *Journal of Applied Physics* **56**, 1838-1840 (1984).
28 Hazen, R. Zeolite molecular sieve 4A: anomalous compressibility and volume discontinuities at high pressure. *Science* **219**, 1065-1067 (1983).
29 Wells, S. A., Leung, K. M., Edwards, P. P. & Sartbaeva, A. Flexibility windows in faujasite with explicit water and methanol extra-framework content. *Dalton Transactions* **44**, 5978-5984 (2015).
30 Lee, Y., Vogt, T., Hriljac, J. A., Parise, J. B. & Artioli, G. Pressure-induced volume expansion of zeolites in the natrolite family. *Journal of the American Chemical Society* **124**, 5466-5475 (2002).
31 Lee, Y. *et al.* Non-framework cation migration and irreversible pressure-induced hydration in a zeolite. *Nature* **420**, 485 (2002).
32 Feng, P. Y., Bu, X. H. & Stucky, G. D. Amine-templated syntheses and crystal structures of zeolite rho analogs. *Microporous and Mesoporous Materials* **23**, 315-322, doi:10.1016/s1387-1811(98)00122-x (1998).
33 Fletcher, R. E., Wells, S. A., Leung, K. M., Edwards, P. P. & Sartbaeva, A. Intrinsic flexibility of porous materials; theory, modelling and the flexibility window of the EMT zeolite framework. *Acta Crystallographica Section B: Structural Science, Crystal Engineering and Materials* **71**, 641-647 (2015).
34 Chatelain, T., Patarin, J., Soulard, M., Guth, J. L. & Schulz, P. Synthesis and characterization of high-silica EMT and FAU zeolites prepared in the presence of crown-ethers with either ethylene-glycol or 1,3,5-trioxane. *Zeolites* **15**, 90-96, doi:10.1016/0144-2449(94)00021-j (1995).
35 Chatelain, T. *et al.* Synthesis of high-silica FAU-, EMT-, RHO- and KFI-type zeolites in the presence of 18-crown-6 ether. *Studies in Surface Science and Catalysis* **105**, 173-180 (1997).
36 Nearchou, A., Raithby, P. & Sartbaeva, A. Systematic approaches towards template-free synthesis of EMT-type zeolites. *Microporous and Mesoporous Materials* (2017).
37 Liu, S. *et al.* Cesium-free synthesis of aluminosilicate RHO zeolite in the presence of cationic polymer. *Microporous and Mesoporous Materials* **132**, 352-356, doi:10.1016/j.micromeso.2010.03.012 (2010).
38 Chatelain, T. *et al.* Synthesis and characterization of high-silica zeolite-rho prepared in the presence of 18-crown-6 ether as organic template. *Microporous Materials* **4**, 231-238, doi:10.1016/0927-6513(95)00009-x (1995).

39 Chatelain, T., Patarin, J., Farre, R., Petigny, O. & Schulz, P. Synthesis and characterization of 18-crown-6 ether-containing KFI-type zeolite. *Zeolites* **17**, 328-333, doi:10.1016/0144-2449(96)00069-3 (1996).
40 Bell, P. & Mao, H. Absolute Pressure Measurements and Their Comparison with the Ruby Fluorescence (R1) Pressure Scale to 1.5 Mbar; Carnegie Institution of Washington Year Book; Carnegie Institution: Washington, DC, 1979. *There is no corresponding record for this reference*, 665-669.
41 Hammersley, A., Svensson, S., Hanfland, M., Fitch, A. & Hausermann, D. Two-dimensional detector software: from real detector to idealised image or two-theta scan. *International Journal of High Pressure Research* **14**, 235-248 (1996).
42 Prescher, C. & Prakapenka, V. B. DIOPTAS: a program for reduction of two-dimensional X-ray diffraction data and data exploration. *High Pressure Research* **35**, 223-230 (2015).
43 Coelho, A. A. TOPAS and TOPAS-Academic: an optimization program integrating computer algebra and crystallographic objects written in C++. *Journal of Applied Crystallography* **51** (2018).
44 Wells, S. A. & Sartbaeva, A. GASP: software for geometric simulations of flexibility in polyhedral and molecular framework structures. *Molecular Simulation* **41**, 1409-1421 (2015).
45 Wells, S. A. & Sartbaeva, A. Template-based geometric simulation of flexible frameworks. *Materials* **5**, 415-431 (2012).
46 Cliffe, M. J. & Goodwin, A. L. PASCal: a principal axis strain calculator for thermal expansion and compressibility determination. *Journal of Applied Crystallography* **45**, 1321-1329 (2012).
47 Yokogawa, K., Murata, K., Yoshino, H. & Aoyama, S. Solidification of high-pressure medium Daphne 7373. *Japanese journal of applied physics* **46**, 3636 (2007).
48 Huang, Y. IR spectroscopic study of the effects of high pressure on zeolites Y, A and sodalite. *Journal of Materials Chemistry* **8**, 1067-1071 (1998).
49 Havenga, E. A., Huang, Y. & Secco, R. A. An investigation of the effect of high pressure on the structure of siliceous zeolite Y. *Materials research bulletin* **38**, 381-387 (2003).
50 Fang, H. & Dove, M. T. Pressure-induced softening as a common feature of framework structures with negative thermal expansion. *Physical Review B* **87**, 214109 (2013).
51 Balestra, S. R. G., Gutierrez-Sevillano, J. J., Merkling, P. J., Dubbeldam, D. & Calero, S. Simulation Study of Structural Changes in Zeolite RHO. *Journal of Physical Chemistry C* **117**, 11592-11599, doi:10.1021/jp4026283 (2013).
52 Knorr, K., Winkler, B. & Milman, V. Compression mechanism of cubic silica sodalite Si12O24 : a first principles study of the Im3-over-bar-m to I4-over-bar-3m phase transition. *Zeitschrift Fur Kristallographie* **216**, 495-500, doi:10.1524/zkri.216.9.495.20347 (2001).
53 Werner, S., Barth, S., Jordan, R. & Schulz, H. Single crystal study of sodalite at high pressure. *Zeitschrift Fur Kristallographie* **211**, 158-162, doi:10.1524/zkri.1996.211.3.158 (1996).
54 Huang, Y. N. & Havenga, E. A. Why do zeolites with LTA structure undergo reversible amorphization under pressure? *Chemical Physics Letters* **345**, 65-71, doi:10.1016/s0009-2614(01)00856-9 (2001).
55 Rutter, M. D., Uchida, T., Secco, R. A., Huang, Y. & Wang, Y. Investigation of pressure-induced amorphization in hydrated zeolite Li-A and Na-A using synchrotron X-ray diffraction. *Journal of Physics and Chemistry of Solids* **62**, 599-606, doi:10.1016/s0022-3697(00)00222-5 (2001).
56 Liu, H. J., Secco, R. A. & Huang, Y. N. Pressure-induced amorphization of hydrated Na-X zeolite. *Physchemcomm*, art. no.-8 (2001).